2012

WIP1 Phage Specificity for B. Anthracis

Sherry Kan

WIP1 PHAGE SPECIFICITY FOR *B. ANTHRACIS*

A Thesis Presented to the Faculty of

The Rockefeller University

in Partial Fulfillment of the Requirements for

the degree of Doctor of Philosophy

by

Sherry Kan

June 2012

WIP1 PHAGE SPECIFICITY FOR *B. ANTHRACIS*

Sherry Kan, Ph.D.

The Rockefeller University 2012

Bacteriophage-based diagnostics and therapeutics have been recognized as tools to combat bacterial infections for nearly a century. Wip1 is a recently isolated phage that infects *Bacillus anthracis*, the notorious biothreat pathogen and gram-positive bacterium that causes anthrax disease. The current standard for identifying suspected *B. anthracis* involves testing for Wγ phage sensitivity. However, studies have shown that the narrow Wip1 host range is even more specific to *B. anthracis* than that of Wγ, suggesting that Wip1 may be a superior diagnostic tool.

Wip1's high specificity to *B. anthracis* is likely mediated by the initial recognition and binding of the virus to the host cell. Most bacteriophages interact with bacterial surfaces using tail fibers, but Wip1 is a tailless phage possessing an icosahedral protein coat covering an internal lipid membrane. These features indicate that Wip1 belongs to the family *Tectiviridae*, a relatively rare phage group with a proposed evolutionary lineage to the mammalian adenovirus. Tectiviruses possess protruding spike complexes at their vertices that are responsible for host recognition and binding.

Based on adsorption assays, we confirmed that Wip1's host range specificity is mediated by its receptor-binding ligand. In order to predict candidate gene products for the Wip1 spike complex, we sequenced the Wip1 genome and conducted extensive genomic analyses with other tectiviral genomes. Observations from subsequent recombinant Wip1 protein expression and purification indicated that Wip1 p23 and p24 form a stable complex. We identified the unique protein Wip1 p23 as a receptor-binding protein using competitive inhibition and antibody neutralization assays. From indirect immunofluorescence microscopy, we also demonstrated that Wip1 p23 binds very specifically to the surface of *B. anthracis*. Finally, we characterized the bacterial receptor for Wip1 as a Sap-dependent cell wall component.

The work in this dissertation has produced a significantly more detailed understanding of Wip1's highly specific tropism for *B. anthracis*. The findings that we report here also demonstrate that Wip1 phage and its receptor-binding ligand p23 are promising, new tools in the detection of *B. anthracis*.

to Derek

ACKNOWLEDGEMENTS

This thesis project would not have been possible without the support of many people. I would like to acknowledge and extend my heartfelt gratitude to the following persons:

- Dr. Vincent Fischetti, my thesis advisor, whose guidance has helped me to accomplish the scientific goals set forth throughout this thesis.
- Dr. Erec Stebbins and Dr. Charles Rice, members of my faculty advisory committee, for their insightful discussions of my research.
- Dr. Richard Calendar, of U.C. Berkeley, for graciously joining my committee as an external member.
- Dr. Nadine Fornelos, for her fruitful collaboration on the genomic analysis.
- All members of the Fischetti lab, for their invaluable help and their camaraderie both inside and outside of lab. I am especially indebted to Dr. Raymond Schuch and Dr. Assaf Raz for their troubleshooting brilliance. I would also like to thank Dr. Assaf Raz and soon-to-be-Dr. Barbara Juncosa for their considerable friendship and encouragement.
- The Rockefeller University Dean's Office (in particular Dr. Sidney Strickland, Dr. Emily Harms, Kristen Cullen, Marta Delgado, and Cristian Rosario), for their support and their continued commitment to providing more career resources for the Rockefeller community.

- All members of my faculty advisory committee and the Dean's office for their exceptional support during my unconventional career exploration.
- Dr. Frank Solomon, of MIT, for his continued mentorship since my undergraduate days.
- My friends and family, for their unquantifiable amount of awesomeness.

TABLE OF CONTENTS

LIST OF FIGURES

LIST OF TABLES

A. LITERATURE REVIEW

1. Introduction

Wip1 (for worm intestinal phage 1) is a recently identified phage that is of great interest for two main reasons. First, Wip1 offers promise as a biodefense tool. It is highly specific against *Bacillus anthracis*, the notorious biothreat agent and gram-positive bacterium responsible for anthrax disease. Host range analysis has demonstrated that Wip1 is even more specific for *B. anthracis* than the current diagnostic standard Wγ phage [1]. Secondly, Wip1 belongs to the family *Tectiviridae*, a relatively rare and unusual group of phage that shares a surprising evolutionary lineage with the mammalian adenovirus. The tectiviral vertex spike complexes are of particular interest for both their structural similarities to adenovirus vertex spikes and their role in host recognition [2-4]. For these reasons, my dissertation focused on characterizing Wip1 phage and, specifically, its vertex spike complex.

2. Bacteriophage

Viruses are obligatory parasites that depend on their host organisms to support replication. Bacteriophage (“eaters of bacteria”), or phage for short, are viruses that infect bacteria and have been reported for more than 140 bacterial genera [5]. Phages are estimated to be the predominant biological entity in the biosphere [6]. They have been isolated from varied environments including oceans [7], Artic sea ice [8], sewage [9], forest soil [1], and the Sahara desert [10]. Phages have evolved to survive harsh conditions such as extreme temperatures up to 95C in hot springs [11] and pH values as low as 1.3 [12].

Bacteriophage were originally discovered independently by Frederick Twort in 1915 and Felix d’Herelle in 1917. After d’Herelle observed that phage titers increased in stool samples from dysentery patients, he recognized the possibility of using bacteriophage as therapeutics [13]. He isolated phages for various bacterial diseases such as cholera, diphtheria, bubonic plague, and anthrax. Many, but certainly not all, early phage therapy trials appeared to be successful, leading to the manufacture and/or marketing of phage preparations by d’Herelle’s laboratory in Paris (today known as L’Oreal) and several pharmaceutical giants (Eli Lilly & Co, Parke-Davis, Squibb & Sons, and Swan-Myers division of Abbott Laboratories, etc.) [13]. Unfortunately, World War II and the discovery of penicillin diverted efforts away from the further development of phage therapy in the United States and Western Europe. Nonetheless, phage therapy trials continued in the former Soviet

Union and Eastern European countries, where phages are still regarded as a viable therapeutic to combat bacterial infections.

Since their discovery, phages have been used as powerful model systems in molecular biology. Phage research has led to many important scientific discoveries [14]. For example, DNA was identified as the hereditary material by Hershey and Chase in 1952 based on studies conducted using bacteriophage T2. In another example, the study of RNA phages in the 1960's provided strong support for Crick's postulated central dogma of molecular biology that information flows from DNA to RNA to proteins. Phages have also been used in practical applications such as phage therapy [13], phage display [15], and diagnosis [16].

There are at least 13 distinct groups of phages classified by the International Committee on Taxonomy of Viruses (ICTV) based on virion morphology and nucleic acid composition. The three groups of dsDNA tailed phages account for 96% of all reported phages in the literature. These three groups differ in their tail morphology – long or short and contractile or non-contractile. The less common phage families exhibit tailless, polyhedral, filamentous, or pleomorphic morphology [6] (Table 1).

Table 1. ICTV classification of bacteriophage

There are 13 families of bacteriophage classified by capsid morphology, nucleic acid composition, and other characteristics such as presence of a tail or an envelope.

Family	Nucleic acid	Characteristics	Morphology
Myoviridae	Linear dsDNA	Non-enveloped, contractile tail	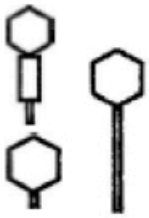
Siphoviridae	Linear dsDNA	Non-enveloped, long non- contractile tail	
Podoviridae	Linear dsDNA	Non-enveloped, short non-contractile tail	
Tectiviridae	Linear dsDNA	Non-enveloped, isometric	
Corticoviridae	Circular dsDNA	Non-enveloped, isometric	
Lipothrixviridae	Linear dsDNA	Enveloped, rod-shaped	
Plasmaviridae	Circular dsDNA	Enveloped, pleomorphic	
Rudiviridae	Linear dsDNA	Non-enveloped, rod-shaped	
Fuselloviridae	Circular dsDNA	Non-enveloped, lemon shaped	
Inoviridae	Circular ssDNA	Non-enveloped, filamentous	
Microviridae	Circular ssDNA	Non-enveloped, isomatric	
Leviviridae	Linear ssDNA	Non-enveloped, isometric	
Cystoviridae	Segmented dsRNA	Enveloped, spherical	

2.1 *Tectiviridae*

The family *Tectiviridae* (from the Latin tectus meaning covered) includes phages possessing an icosahedral protein shell covering an inner membrane bilayer containing a linear dsDNA genome. A relatively rare phage group, the family currently consists of six isolates that infect gram-negative bacteria and six that infect gram-positive bacteria. Gram-negative infecting tectiviruses include PRD1 [9] and five closely related phages: PR3 [17], PR4 [18], PR5 [19], PR772 [20], and L17 [21]. Gram-positive infecting tectiviruses include Bam35 [22], AP50 [23], phiNS11 [24], GIL01 [25], and GIL16 [26], and Wip1 [1].

The majority of bacteriophages have a single central tail fiber that is used to penetrate the bacterial cell wall and deliver the viral genome. In contrast, tectiviruses are tailless and possess 11 labile vertices capable of host binding and DNA delivery [3]. The twelfth vertex is proposed to play a role in DNA packaging instead of receptor binding. All sequenced tectiviruses have been shown to encode two different lytic enzymes. A proposed model suggests that one lysin is a structural component of the virion active against the peptidoglycan during genome delivery while the second lysin is responsible for host cell lysis and progeny liberation following genome replication and virion production [27].

2.1.1 PRD1

PRD1 is the best characterized member of the *Tectiviridae* family and infects a broad range of gram-negative bacteria including *Escherichia coli* and *Salmonella enterica* [28]. The tailless, icosahedral, inner membrane-containing phage possesses a 14,925 bp linear dsDNA genome with covalently linked terminal proteins [9]. One-step growth experiments indicated that the latent period was about 50 minutes and the burst size is roughly 500 infective particles per cell [29]. The PRD1 virion measures 70 nm in diameter and its genome shares approximately 98% sequence identity with other gram-negative infecting tectiviral isolates (PR3, PR4, PR5, and L17). Additionally, PRD1 surprisingly shares many striking structural similarities to and a proposed common evolutionary lineage with the mammalian adenovirus [30, 31]. Both viruses share a similar overall architecture, with comparably structured capsid lattices and spike complexes at their vertices.

Through crystallization and mutagenesis studies, PRD1 proteins have been fairly well defined. The capsid is stabilized by pentameric glue protein P30 and hexameric major coat protein P3. Pentameric vertex protein P31 occupies each of the twelve vertices and forms the base of the spike complex. Two elongated proteins, trimeric spike protein P5 and monomeric receptor binding protein P2, form two separate spikes that protrude from P3 [2, 32, 33] (Figure 1). The presence of P2 is dependent on P5, while both P2 and P5 are missing in mutants lacking P31 [3].

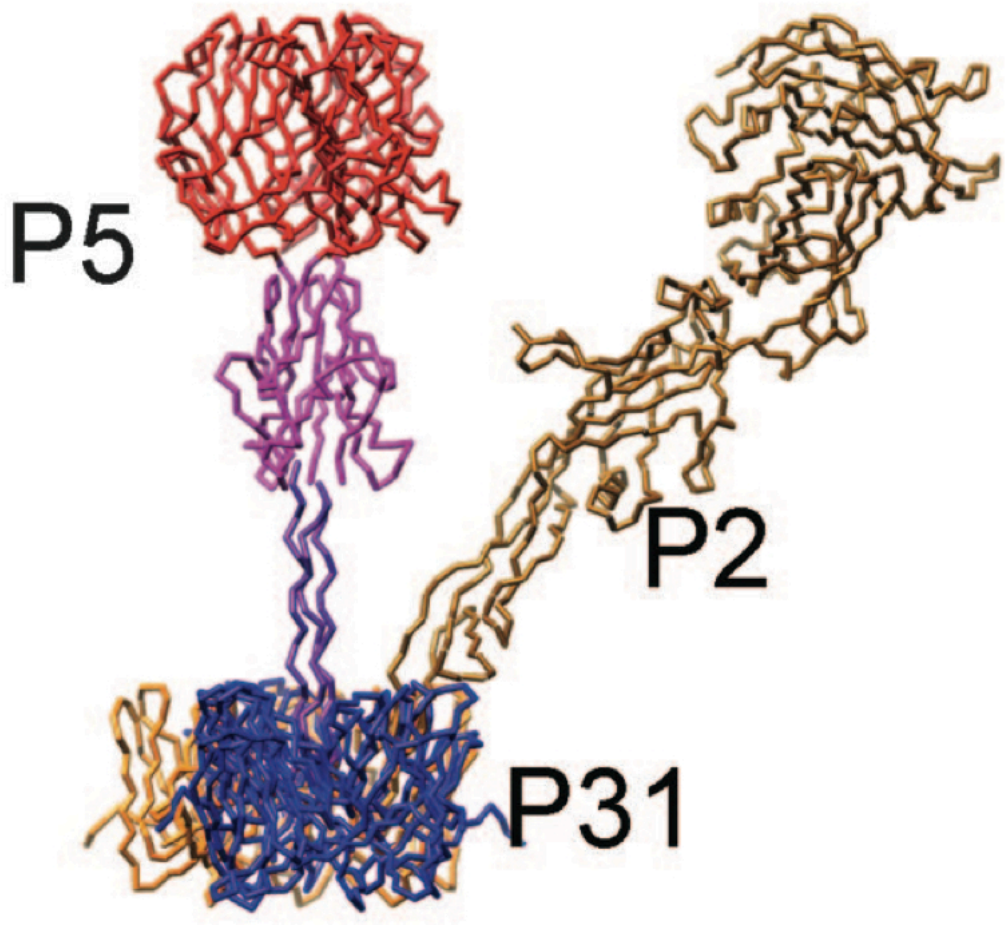

Figure 1. Model for the PRD1 spike complex shown from the side

The PRD1 spike complex is composed of pentameric vertex protein P31, trimeric spike protein P5, and monomeric receptor-binding protein P2. In this representation of the protein structures, one P5 monomer (represented in red, purple, and blue), one P2 monomer (represented in brown), and one P31 monomer (represented in orange) are modeled.

The X-ray structure for receptor binding protein P2 resembles an elongated sea horse with a distinct B propeller head and tail with a protruding proline-rich fin (Figure 1). Receptor binding is likely to occur through the head, which is distal to the virion. In one P2 model, the fin-shaped domain is proposed to make initial contacts by scanning the host surface in order to bring the head domain close to its receptor [4]. In another P2 model, the fin-shaped domain is suggested to interact with the rest of the spike complex.

Interaction of protein P2 with the receptor leads to a conformational change that results in the dissociation of the metastable spike complex proteins from the virion [32]. This is followed by the transformation of the spherical internal membrane into a tube-like channel structure for the delivery of viral DNA into the host [33, 34]. The genetic material is released into the bacterial cell, while the empty phage capsid remains outside [35]. In P2-mutants, tube-like channels spontaneously form and release DNA, indicating that P2 is also responsible for stabilizing a metastable vertex structure [32].

2.1.2 Bam35

Bam35 is a tectivirus that infects gram-positive *Bacillus thuringiensis* [22]. Based on negative-stain electron microscopy and electron cryo-microscopy with 3-D image reconstruction, the morphology of 73 nm Bam35 virions was shown to closely resemble that of PRD1 [36, 37] (Figure 2). Similar tube-like membrane structures have also been observed for Bam35 upon host

binding [36, 37]. While wild-type Bam35 form turbid plaques, an isolate designated Bam35c yielded clear plaques and higher propagation titers. The 14,935 bp linear dsDNA molecule of Bam35c is covalently linked to terminal proteins. The Bam35c genome exhibits a similar organization and size as the PRD1 genome, but no detectable sequence similarity [37]. On the other hand, the Bam35 genome shares high sequence similarity with GIL01 and GIL16, tectiviruses that also infect *B. thuringiensis* [25, 26, 38]. Genomic analysis predicted 32 open reading frames (ORFs), all on the positive strand, in a tightly packed organization with numerous overlapping ORFs [37].

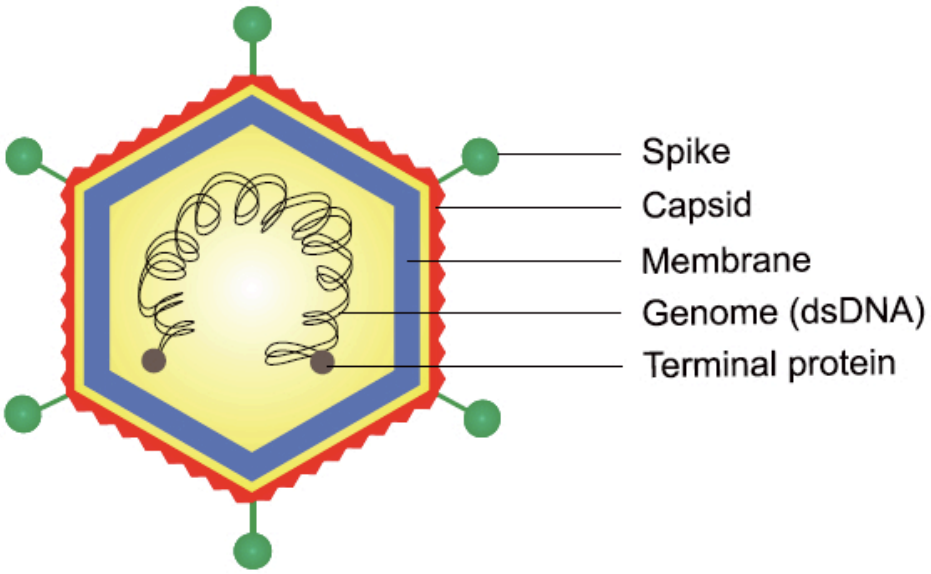

Figure 2. Schematic of the Bam35 virion

Bam35 gene products gp27, gp28, and gp29 have been identified as candidate proteins for the spike complex. Genomic analysis of the organizational location of ORF27 suggested that it is the vertex penton protein of the spike complex. By threading Bam35 proteins onto PRD1 X-ray structures, it was determined that gp28 is homologous to spike protein P5 and that gp29 is homologous to the C-terminal half of receptor binding protein P2 [36, 37]. In addition, gp28 and gp29 were determined to reside on the surface of Bam35 from phage aggregation and neutralization assays using polyclonal antibodies [39]. However, competitive binding assays using both recombinant and dissociated surface proteins were inconclusive and a Bam35 receptor binding protein could not be identified.

Bam35 was found to rapidly adsorb to the peptidoglycan layer of the host with signs of receptor saturation at an MOI of approximately 600 virions per one cell [39]. Studies demonstrated that one of the two major sugar components of the peptidoglycan, N-acetyl-muramic acid, neutralized the virus and thus was proposed to be a receptor for the phage [39]. Upon host adsorption, Bam35, like gram-negative infecting PRD1, displayed tube-like membrane structures that are hypothesized to deliver the genome into the cytosol. Based on electron microscopy, mature virus particles accumulate at the center of the infected host at about 40 minutes post infection. Lysis occurs at roughly 45 minutes post infection and takes 15 minutes to complete before releasing roughly 39 infective particles per cell [37].

2.1.3 GIL01 and GIL16

GIL01 and GIL16 are both *B. thuringiensis* phages with similar morphologies to other tectiviruses, characterized by a tailless, icosahedral capsid measuring about 60 nm and containing an inner lipid membrane. GIL01, an isolate from *B. thuringiensis* serovar Israelensis, shares 99% sequence identity with Bam35, which was isolated from *B. thuringiensis* serovar Alesti. Their genomes differ by only 11 bp and none of the mutations significantly alter the genetic organization of either phage, suggesting that GIL01 and Bam35 are virtually the same [26]. GIL01 shares 83.6% sequence identity with GIL16, an isolate from *B. thuringiensis* B16. Studies showed that GIL01 and GIL16 have slightly different host ranges. Interestingly, GIL01 does not infect *B. thuringiensis* serovar Thuringiensis HER1047, a strain that is susceptible to both Bam35 and GIL16 [26].

2.1.4 AP50

AP50 is a tectivirus isolated from soil in 1972 that specifically infects *B. anthracis*. TEM analysis revealed a shell composed of two layers displaying icosahedral symmetry and SDS-PAGE gels revealed nine major structural proteins. Organic solvents such as chloroform and ether inactivated AP50, confirming the phospholipid natures of the inner layer [40]. Burst size was temperature dependent, with 200 to 300 particles per cell released at 25^{o}C and 37^{o}C compared to about 3 to 5 particles per cell at 42^{o}C. Originally

thought to contain RNA [23], it has now been determined to possess a 14,398 kbp linear dsDNA genome encoding 31 putative ORFs [41].

Wild-type AP50t produces turbid plaques, while the spontaneous variant AP50c produces clear plaques. Interestingly, there exist only two sequence changes between the two genomes. One mutation is located in the non-coding region just upstream of ORF1. The other mutation is located within ORF28, which has been designated a highly variable region of the genome [41]. While Bam35, GIL01, and GIL16 share 86 to 99% sequence identity, AP50c is less closely related to these other gram-positive infecting tectiviruses with only ~53% overall percent identity.

Wild-type AP50t was shown in 1977 to have a very narrow host range, infecting only one-third of the 34 *B. anthracis* strains and none of the 52 *B. cereus* strains tested [42]. Recently, mutant variant AP50c was also shown to be highly specific to *B. anthracis* in an even more extensive host range analysis. 111 of the 115 *B. anthracis* strains and none of the 100 *B. cereus* sensu lato strains were susceptible to AP50c infection [41].

2.1.5 Wip1

Wip1 is a recently identified phage isolated from the intestinal tract of *Eisenia fetida* earthworms in 2003 [1]. The earthworms were taken from forest floor soil in Stroudsburg, Pennsylvania. Wip1 is a tailless phage with an isometric head belonging to the family *Tectiviridae* (Figure 3) and produces tube-like structures after adsorption or chloroform treatment [43].

Wip1 exhibits a very narrow host range and is highly specific to the notorious pathogen *B. anthracis*. The current gold standard for identifying suspected *B. anthracis* involves testing for Wγ phage sensitivity [16]. However, using Wγ as a diagnostic tool can lead to false positives due to the susceptibility of several *Bacillus cereus* strains to infection by this phage. Recent studies have shown that the host range of Wγ is less specific to *B. anthracis* than that of both Wip1 and AP50 [1, 41]. For example, *B. cereus* strain ATCC 4342 is sensitive to infection by Wγ phage but not to infection by either Wip1 or AP50. Additionally, the Wγ diagnostic phage yields plaques on *B. anthracis* ΔSterne only after 5 days, whereas Wip1 plaques can be detected after just 12 hours post infection [1]. These advantages suggest that Wip1 may be a superior diagnostic tool to Wγ.

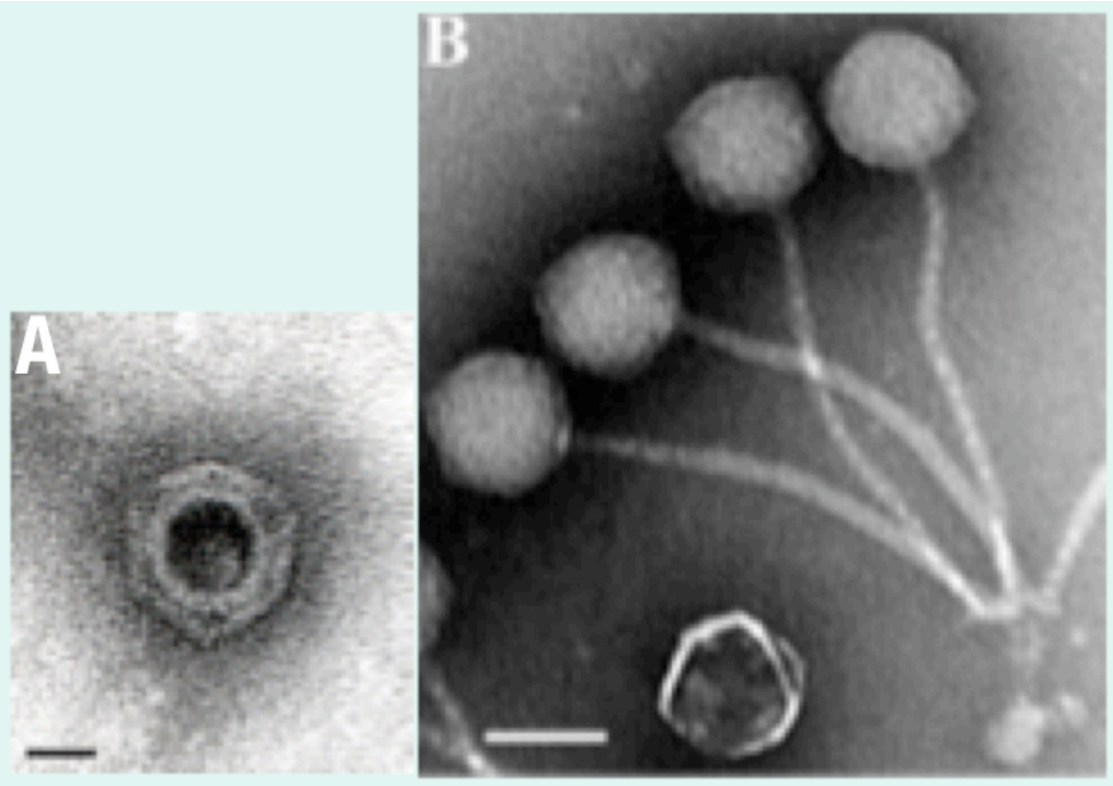

Figure 3. Comparison of Wip1 and Wγ phage morphologies

A. TEM of Wip1 phage. Scale bar = 25 nm

   Wip1 phage belongs to the family *Tectiviridae*, characterized by a tailless icosahedral protein capsid surrounding an inner lipid membrane. The Wip1 vertex to vertex dimension measures about 60 nm.

B. TEM of Wγ phage. Scale bar = 50 nm

   Wγ phage belongs to the family Siphoviridae, characterized by an icosahedral head with sheathless, non-contractile, long tails. Wγ heads measure 52 nm and their tails measure 185 nm long and 9.5 nm wide.

2.2 Adsorption

Specificity of a bacteriophage host range is often mediated by specificity of adsorption. Receptor-binding proteins on the coat of the phage interact very specifically with receptors exposed on the surface of the bacterium. Since phage lack independent mobility, adsorption results from random phage-cell collisions. It was suggested by Adam and Delbruck that adsorption occurs in two stages [44]. In order to efficiently bind to a receptor, which is small compared to the overall size of a cell, the phage particle first finds the bacterial surface by 3D diffusion involving reversible binding to a general recognition molecule. Once on the cell surface, the phage particle then diffuses in a 2D fashion until it collides with a specific receptor, which it binds to irreversibly. For the two-stage capture model to be advantageous, the affinity between the host surface and the phage must be strong enough so that the phage remains on the surface yet weak enough so that it can diffuse across the surface [45]. While Adam and Delbruck's theory assumed that all collisions lead to binding, more recent studies have observed that that the second irreversible binding step is surprisingly inefficient with only a small fraction of the collisions leading to actual irreversible binding [46].

2.2.1 Bacteriophage receptor binding proteins

The adsorption of phages to the host receptors is mediated by receptor-binding proteins on the surface of the viral particle. Most receptor-binding

ligands are homomultimeric complexes that are involved with functions such as cell wall penetration or DNA delivery in addition to host recognition. While the domains that attach receptor-binding sites to the virion surface tend to be well conserved among the members within a phage group, the receptor-binding domains are usually encoded in highly variable regions and tend to display more sequence diversity.

The phages p2, bIL170, and TP901-1 are siphoviruses that infect the bacterium *Lactococcus lactis*, used extensively worldwide for manufacturing fermented milk products. The crystal structures of the receptor binding proteins for these phages have been resolved. Despite lack of sequence similarity and differences in host range within *L. lactis*, the three RBP structures are remarkably close [47]. Each is postulated to be a homotrimer located at the tip of their long, flexible, non-contractile tail and binds to unknown surface saccharides [48]. Additionally, recent X-ray crystallography studies showed that p2's RBP also shares significant structural similarity with siphovirus SPP1's gp22 [49]. This viral protein is hypothesized to form the tip of the tail of SPP1, a phage that infects *Bacillus subtilis* using receptor protein YueB.

Podoviruses bind to cell hosts using stubby tail spikes attached to a very short, non-contractile tail. Three to six tail spikes are required for infectivity and the receptor-binding site is centrally located on the tail spike. The tail spike of podovirus P22 is a stable homotrimer that exhibits both binding and hydrolytic cleaving activity against *Salmonella* cell surface O-

antigen polysaccharide [50]. Another podovirus K1-5 has evolved to encode two different tail spike proteins, one to bind type K1 and the other to bind type K5 *Escherichia coli* strains [51]. Curiously, based on high sequence and structural homology, it has been suggested that *Podoviridae* and *Myoviridae* exchange receptor-binding domains [52].

E. coli phage T4 belongs to the family *Myoviridae* and adsorbs to the host surface using both long and short tail fibers. First, the receptor-binding tip of the long tail fibers reversibly interacts with lipopolysaccharides or outer membrane porin protein C. Upon adsorption with at least three long tail fibers, homotrimeric short tail fibers extend and irreversibly bind to the outer core region of the lipopolysaccharides. The T4 long tail fibers are a complex of four different proteins and possess a receptor-binding tip that is highly homologous to the tip of the bacteriophage lambda side tail fibers [53].

PX174 is a tailless icosahedral phage with protruding adsorption spikes consisting of five G proteins and one H protein. Protein G exhibits a significantly higher affinity to *E.coli* lipopolysaccharide (LPS) than protein H towards the same LPS. Spike protein G was also found to form a star-shaped pentamer that provides a channel for DNA delivery. Lastly, studies showed that protein G recognizes both the polysaccharide and lipid regions of gram-negative LPS [54].

Membrane-containing phages such as PRD1, PM2, and p6 bind to receptors using spike proteins. Tectivirus PRD1 has two separate spikes,

trimeric spike protein P5 and receptor-binding protein P2, protruding from its vertices [2]. P2 is required for both adsorption and stabilization of the labile spike complex. Corticovirus PM2 has a pentameric receptor-binding protein P1 occupying each vertex. The crystal structure of P1 revealed a Ca2+ ion bound in a cleft at the tip of the protein that may mark the site of sugar binding [55]. Cystovirus p6 binds to its receptor using spike protein P3.

2.2.2 Gram-positive cellular receptors

The cell wall of gram-positive bacteria differs significantly from that of gram-negative bacteria in both composition and structure. Gram-positive bacteria typically lack an outer membrane and possess a considerably thicker cell wall due to a thick peptidoglycan layer. Peptidoglycan is a heteropolymer composed of sugars and amino acids that forms a cross-linked mesh-like layer outside the plasma membrane. Gram-positive cells also have cell wall glycopolymers attached to the peptidoglycan or cytoplasmic membrane, such as teichoic acids, teichuronic acids, arabinogalactans, lipoteichoic acids, lipomannans, and lipoarabinomannas. These cell wall glycopolymers constitute the bulk of bacterial surface antigens and anchor the crystalline surface layer (S-layer) proteins to the cell wall.

Phage receptors localized on the cell wall of gram-positive bacteria can include peptidoglycan, teichoic acids, membrane-anchored proteins, or cell wall-linked polysaccharides. N-acetyl-muramic acid, a major component of

peptidoglycan, was identified as a component of the *B. thuringiensis* receptor for tectivirus Bam35 [39]. Peptidoglycan was shown to bind to gram-positive infecting phages sk1, jj50, and 64 [56]. Teichoic acid has been identified as the *B. subtilis* receptor for bacteriophage SP50, but additional cell wall constituents are also believed to be involved in the interaction [57]. Bacteriophages p25 and p29 attach to teichoic acid components, while *lactobacillus* phages LL-H and JCL1032 adsorb to lipoteichoic acid elements [58]. Teichoic acids are the surface component involved in initial reversible binding of phage SPP1 to host cells, followed by irreversible adsorption to the ectodomain of *B. subtilis* protein YueB [59, 60].

The *B. anthracis* receptor for Wγ phage was identified as LPXTG protein GamR [61]. The protein receptor was discovered based on the observation that sortase deficient *B. anthracis* was not as sensitive as the parent strain to Wγ binding and infection. Interestingly, both Wγ sensitive *B. cereus* ATCC 4342 and Wγ resistant *B. thuringiensis* 97-27 possess very similar Gam-R like proteins with 89% and 96% homology, respectively [61]. Electron microscopy showed that Wγ phage bound to both strains [61]. These observations revealed that GamR is sufficient for virion binding but not for DNA delivery into *B. thuringiensis* 97-27. This suggests that there is a putative second receptor necessary for DNA delivery, a cell wall component absent on the surface of *B. thuringiensis* 97-27.

3. *Bacillus anthracis*

Bacillus anthracis is a gram-positive, rod-shaped, non-motile, spore-forming bacterium with a width of 1-1.2 μm and a length of 3-5 μm. It can be cultured in ordinary nutrient medium with iron sources under either aerobic or anaerobic conditions. It is also one of the few bacteria known to synthesize an antigenic capsule consisting of a poly-D-glutamate polypeptide. *B. anthracis* was the first bacterium demonstrated to cause disease. In 1850, Rayer described filiform bodies in the blood of animals dying from anthrax. In 1863, Davaine showed that anthrax disease could be transmitted from animal to animal by injection with infected blood. In 1877, Koch injected cultured *B. anthracis* into animals and generated experimental anthrax disease. A few years later, Pasteur successfully attenuated *B. anthracis* and used the attenuated strains to vaccinate sheep against fully virulent strains.

B. anthracis is both genotypically and phenotypically similar to *Bacillus cereus*, a ubiquitous soil inhabitant, and *Bacillus thuringiensis*, an insect pathogen. The *Bacillus* family's distinguishing feature is the production of endospores, which are highly resilient, dormant, temporary structures formed within the cells. These spores are cryptobiotic with no detectable metabolism. *B. anthracis* spores are particularly durable and can survive environmental stresses such as high temperatures, low-nutrient conditions, irradiation, strong acids, disinfectants, and other harsh physical conditions for decades or centuries.

Analysis of 16S and 23S rRNA has shown that *B. anthracis* has remarkably close relationships with *B. cereus* and *B. thuringiensis*. The *B. anthracis* 16S rRNA shares 100% sequence identity with that of *B. cereus* and their 23S rRNA sequences differ by only two nucleotides. *B. anthracis* is also very similar to *B. thuringiensis*, with only nine nucleotides differing between their respective 16S rRNA sequences [62]. Notably, *B. anthracis* is even more similar within itself. In fact, it may be one of the most molecularly homogenous bacteria known with shared genetic similarities of over 90% between different *B. anthracis* strains and isolates.

3.1 Anthrax disease

Bacillus anthracis is the causative agent of anthrax, a severe disease that can infect any mammal, including humans. It predominantly infects domesticated and wild animals, especially herbivores (including cows, sheep, and horses). However, humans can become infected through contact with diseased animals or as a result of bioterrorism. In the United States, there are 1-2 cases per year of naturally acquired anthrax in humans [63]. In September and October of 2001, lethal *B. anthracis* spores were used to deliberately contaminate envelopes sent through the mail. This bioterrorism attack led to 22 infections and five deaths from inhalation anthrax [63]. Today, the Center for Disease Control and Prevention continues to classify anthrax as a highest priority Category A agent with recognized biowarfare potential.

B. anthracis can cause three types of infections: cutaneous, gastrointestinal, and inhalational. A cutaneous infection, usually the result of a cut or abrasion, is the most common and least dangerous infection type with a mortality rate of less than 1% [64]. A gastrointestinal infection, usually the result of eating infected meat or drinking contaminated water, is frequently seen in carnivores. The inhalation of *B. anthracis* spores results in bacterial germination and colonization of the host's mediastynal lymph nodes. As the capacity of the lymph nodes is exceeded, the bacteria enter the host's blood stream and cause septicemia. The most dangerous of the three types of infection, *B. anthracis* inhalation is almost invariably fatal with a near 100% mortality rate if not treated within 24-48 hours of contact [64].

The early clinical diagnosis of inhalation anthrax is extremely challenging since the initial symptoms mimic that of influenza. Within 2-3 days, patients progress from flu-like myalgias, fever, and malaise to dramatically more severe symptoms such as dyspnea and hypoxemia, followed by hypotension, hemorrhage, and death [65]. *B. anthracis* is susceptible to the antibiotic penicillin, but resistant β-lactamase-positive strains have been isolated. Alternative antibiotic drugs include ciproflaxin, erythromycin, tetracycline, doxycycline, and chloramphenicol [65].

Fully virulent strains of *B. anthracis* harbor two endogenous plasmids, pXO1 and pXO2. pXO1 encodes three toxins that are responsible for the majority of pathology associated with *B. anthracis* while pXO2 codes for the

protective capsule. The attenuated Sterne strain has only one plasmid pXO1 and the avirulent ΔSterne strain has neither plasmid.

3.2 *Bacillus anthracis* detection

The dissemination of *B. anthracis* spores in a bioterrorist attack continues to be a serious concern. A rapid, accurate, and sensitive detection method would be a valuable tool for identifying whether *B. anthracis* is the agent of an attack, especially because infection is difficult to diagnose and anthrax has a high mortality rate. However, reliable identification of *B. anthracis* is difficult due to its remarkable similarities to *B. cereus* and *B. thuringiensis*.

B. anthracis can be identified using basic characterization assays. It is sensitive to penicillin, non-motile, and not β-hemolytic on sheep or horse blood agar plates. The current standard for *B. anthracis* identification is lysis by Wγ phage. Originally isolated in 1955 by Brown and Cherry, Wγ was found to lyse encapsulated smooth forms of *B. anthracis* but not any *B. cereus* strains that were tested at the time. Later studies have identified two sensitive non-*B. anthracis* strains, *B. cereus* ATCC 4342 and *B. mycoides* CDC680, as well as two nonsusceptible *B. anthracis* strains [16]. Additionally, the Wγ lysin PlyG was found to lyse *B. anthracis* is a highly rapid and specific manner and could be developed as a tool to quickly detect germinating Wγ sensitive spores [66].

Immunoassays using antibodies against *B. anthracis* spores, vegetative cells, and toxin proteins have also been developed to detect *B. anthracis*. Immunofluorescence systems, ELISA assays, and immunoradiometric assays can detect spore surface antigens that are specific to *B. anthracis* using immobilized spores. Some immunoassays, such as serological detection and monoclonal antibodies against vegetative cell surface antigens, suffer from cross-reactivity [67]. Others, such as sandwich-based antibody arrays and flow cytometry to detect fluorescein-labeled antibodies to spores, have detection limits. There are also enzyme immunoassays that detect anthrax toxins in the blood, but these require the disease to have already progressed to an advanced stage [67].

B. anthracis can also be detected using DNA-based assays. The United States Postal Service had previously installed real-time PCR based anthrax screening units at select sorting sites. PCR, real-time PCR, and multiplex PCR techniques are based on amplification of *B. anthracis* specific DNA. Most primers are designed to target sequences on either or both of the virulence plasmids, pXO1 or pXO2. Studies have also identified a 277 bp region of the chromosome that is conserved in 28 *B. anthracis* strains tested, but could not be found in 33 heterologous bacteria strains [67]. However, this target is not indicative of virulence and was later found in several *B. cereus* and *B. thuringiensis* strains. Newer methods of DNA-based *B. anthracis* detection do not require amplification steps such as PCR. Instead, the nucleic acid is

detected using a sandwich-hybridization assay with a fluorophore-labeled probe [67].

3.3 *Bacillus anthracis* surface layer

The *B. anthracis* cell wall differs from other gram-positive cell walls in that they do not contain teichoic acid, a major cell wall component and popular phage receptor in other gram-positive strains, and their surface layers are not glycosylated. Furthermore, the cell wall contains carbohydrate residues that are specific in composition to *B. anthracis* and different from that of even closely related *B. cereus* strains [68]. Virulent *B. anthracis* also forms a poly-D-glutamate capsule. However, *B. anthracis* ΔSterne, the strain mainly used in this study, does not harbor the virulent plasmids and thereby does not possess a protective capsule.

Bacterial S-layers are two-dimensional sheets of protein that self-assemble on the cell surface. In *B. anthracis* ΔSterne, S-layers are the outermost interaction zone with their respective environment (Figure 4). The main S-layer proteins of *B. anthracis* are Sap and EA1, which are encoded by the clustered genes sap and eag, respectively [69]. The gene csaB lies adjacent to this operon, is responsible for the pyruvylation of the secondary cell wall carbohydrates that S-layer proteins are anchored to, and is required for the retention of S-layer proteins on the cell wall [70].

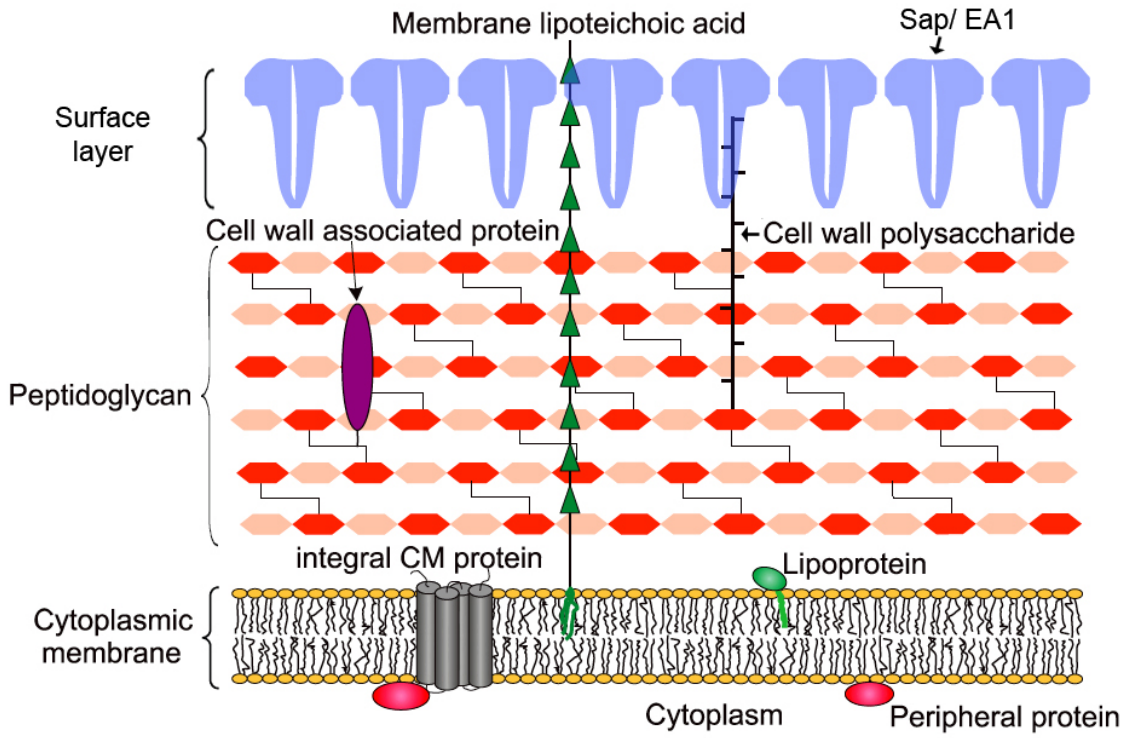

Figure 4. Schematic of the *B. anthracis* ΔSterne cell wall

The cell wall of gram-positive *B. anthracis* ΔSterne has a thick peptidoglycan layer composed of cross-linked sugars and amino acids. Major components associated with the cytoplasmic membrane and peptidoglycan include membrane lipoteichoic acids, cell wall proteins, and cell wall polysaccharides. These associated glycopolymers anchor the crystalline surface layer Sap and EA1 proteins to the cell wall. The *B. anthracis* cell wall differs from other *Bacillus* strains in that it lacks teichoic acids and S-layer glycosylation. *B. anthracis* ΔSterne lacks the plasmid that encodes the virulent capsule.

In *B. anthracis*, Sap and EA1 are sequentially produced under growth phase control. Studies have suggested that an exponential phase Sap layer is subsequently replaced by a stationary phase EA1 layer [71]. In part, this regulation is due to recognition of the *sap* promoter by SigA, the housekeeping sigma factor for RNA polymerase, and recognition of the *eag* promoter by SigH, a transition state regulator that quadruples in concentration at the onset of stationary phase [71]. This regulatory mechanism is highly flexible, as shown by the observation that Sap is readily expressed if stationary phase cells are resuspended in fresh medium.

4. Objectives of the Study

The goal of this study was to develop a better understanding of Wip1's highly specific tropism for *B. anthracis* by studying the spike complex. We started by imaging the morphological changes of Wip1 phage upon adsorption, expanding its host range analysis with adsorption studies, and sequencing its viral genome. Based on genomic analysis comparing the Wip1 genome with that of other gram-positive infecting tectiviruses, candidate gene products for the Wip1 spike complex were predicted and used to identify a Wip1 receptor binding protein that detects and exhibits specificity for *B. anthracis*.

B. MATERIALS AND METHODS

1. Bacterial strains and phages

The majority of bacterial strains in the present study have been previously described [1, 43, 66]. All bacterial strains were grown in brain heart infusion (BHI; Remel) broth or agar plates at 30^{o}C according to standard protocols. The bacteriophage Wip1 was isolated from the intestinal tract of *Eisenia fetida* worms from Pennsylvania, USA. Phage propagation was performed on the *B. anthracis* ∆Sterne strain.

2. Phage propagation

High titer phage stocks were obtained by infecting stationary cell cultures (100 µl) with 100 µl of a series of diluted (1:100 to 1:1000) Wip1 phage stocks. The phage-bacterium mixtures were incubated in a 37^{o}C waterbath for 15 min and then plated with molten top agar (0.8%) onto BHI plates and incubated overnight at 30^{o}C. When the viral plaques reached near confluency, the soft agar overlays were collected in conical tubes, incubated with 2 ml 10 mM K phosphate per plate for 15 min at room temperature, and centrifuged at 4,000 rpm for 20 min at 4^{o}C. The resulting supernatants were filtered (0.45-µm-pore-size-filter) and stored at 4^{o}C.

3. Phage purification scheme

High titer stocks of 1E9 – 1E10 PFU/ml Wip1 phage were produced and filtered. Thee stocks were precipitated using PEG8000 and then concentrated 10X by centrifugation (Sorvall GS-3; 8,000 rpm; 30 min; 4^{o}C). Phage pellets were resuspended in 10 mM KPhosphate. Step gradients of CsCl layers were overlaid with concentrated phage and centrifuged (Ti40 rotor; 22,000 rpm; 3 h; 4^{o}C). Bands were extracted using both needle puncture and fraction removal by pipette. Alternately, concentrated phage stocks were also overlaid on continuous sucrose gradients of 20 – 70% that were centrifuged (Ti40 rotor; 22,000 rpm; 24 h; 4^{o}C). Bands were extracted by pipette removal of fractions. The gradient fractions containing the phage bands were dialyzed against 10 mM K Phosphate at 4^{o}C and then titered on *B. anthracis* ΔSterne to test for activity.

4. Transmission electron microscopy

Wip1 phage were incubated with overnight cultures of *B. anthracis* ΔSterne at a MOI of 10 for 5 min at 37^{o}C. After incubation, the mixtures were transferred to a new microfuge tube with solidified agar on the bottom to act as a cushion during the subsequent centrifugation at 6000 rpm for 3 min. Supernatant was removed and the pellet was resuspended in 1x fixative. The TEM analyses were then performed at The Rockefeller University Bio-Imaging Resource Center as previously described [43].

5. Chloroform sensitivity assay

Wip1 phage samples (2 ml) were incubated with and without various volumes of chloroform (up to 80 µl) in capped glass tubes with gentle mixing at room temperature for 15 min. The mixtures were then titered on *B. anthracis* ΔSterne. W2 phage with and without chloroform plated on *B. cereus* ATCC 4342 was used as a control.

6. Phage adsorption assay

Various bacterial strains were grown to stationary phase (approximately 2 x 10^8 CFU/ml) and 100 µl of bacteria was mixed with 100 µl of Wip1 at 2 x 10^7 PFU/ml. The phage-bacterium mixtures were incubated in a 37^{o}C waterbath for 20 min and then pelleted at 7000 rpm for 3 min. The resulting supernatants were subsequently spin-filtered (Millipore; 0.22 µm) and titered on plates of *B. anthracis* ΔSterne.

7. DNA manipulation and sequencing

To obtain Wip1 DNA, Wip1 phage stock was lysed using NaOH and then neutralized with Tris buffer and water. Tsp5091-digested restriction fragments of mixed population were ligated to linkers, PCR amplified, and inserted into TOPO vectors. After transforming these mixed plasmids into a library of One Shot TOPO competent cells, uniform plasmid preparations were

extracted and sequenced. Sequences derived from these transformed cells were aligned to form a contiguous sequence using DNAStar Lasergene Seqman Pro software. The final contig exhibited 11X average coverage and was confirmed by sequencing PCR products generated directly from Wip1 phage DNA.

8. DNA purification

In order to extract purified DNA from Wip1, high titer phage stocks were first concentrated using direct centrifugation (UC 35K rotor; 30,000 rpm; 6 h; 4^{o}C). The pellet was resuspended in 1/100 original volume of 10 mM K Phosphate buffer. To remove viral coat proteins, 1/5 resuspension volume of 10% SDS and 1/5 resuspension volume of 10 mg/ml protease K were added and the reaction was incubated at 55^{o}C for 1.5 h. Organic solvents were then used to disrupt the lipid membranes and separate phage DNA through 5X phenol extractions followed by 2X chloroform extractions. The DNA in these solutions was ethanol precipitated, washed in 75% ethanol, and finally resuspended in 1/1000 original volume of ddH2O. The extracted DNA was verified by PCR using primers specific to Wip1.

9. DNA-terminal protein analysis

To test for the presence of covalently linked terminal proteins, the purified DNA was subjected to further protease K treatment followed by multiple phenol and chloroform extractions, ethanol precipitation and washes, and resuspension in ddH2O. The conditions for these steps are outlined above in the DNA purification methods. DNA samples with and without this second round of protease K treatment were analyzed using gel electrophoresis.

10. Lysogen induction assay

A lysogenic strain of *B. anthracis* ΔSterne harboring a Wip1 prophage was tested for induction by UV irradiation. Overnight cultures of the lysogen were inoculated in BHI and grown to exponential phase for 3 h shaking at 30^{o}C. These cells were pelleted and resuspended in 5 ml of 10 mM MgSO4 and transferred into an uncovered dish. This dish of cells was irradiated with a 254 nm lamp from above at a distance of about 10 cm for 10 seconds. The cells were then incubated at 37^{o}C shaking at 200 rpm for 15 min. Once again, they were pelleted and resuspended in liquid BHI media. Phage induction was allowed to proceed for 90 min at 37^{o}C shaking at 200 rpm before culture supernatants were recovered and filtered (0.45 μm). Filtered supernatants from both irradiated and non-irradiated cells were titered on *B. anthracis* ΔSterne in BHI plates.

11. Cloning of his-tagged Wip1 ORFs 22, 23, and 24

Standard molecular-cloning techniques were performed as described by Sambrook and Russel. The PCR products containing the coding sequences for the Wip1 gene products 22, 23, and 24 were separately amplified using specific primers. Each DNA fragment was inserted into a modified CDFDuet-1 plasmid between the SalI-NotI sites preceded by a T7lac promoter and ribosome binding site as well as two sets of His-tag sequences. Clones were confirmed by sequencing using primers that flank the insert.

12. Purification of his-tagged Wip1 p22, p23, and p24

Overnight cultures of *E. coli* DH5alpha cells carrying the cloned constructs were diluted 1:100 and grown in LB medium with spectinomycin (20 µg/ml) for 4 h while shaking at 37^{o}C. After being moved to 16^{o}C, the cultures were induced with isopropyl-b-D-thiogalactopyranoside (IPTG) at a final concentration of 0.25 mM and shaken for an additional 18 h. Bacterial pellets were collected by centrifugation (Sorvall SLC-6000 rotor; 7200 rpm; 30 min; 4^{o}C) and resuspended in a cold buffer (50 mM Tris, pH 8.0 + 200 mM NaCl + 5 mM imidazole) at 1/100 of the original culture volume. Bacterial lysis was conducted by multiple passages through a French pressure cell (at ~105 MPa) at 4^{o}C. The cell debris was removed by centrifugation (Sorvall SS-34 rotor; 8,000 rpm; 20 min; 4^{o}C) followed by filtration (Nalgene; 0.45 µm).

The following purification steps were conducted at room temperature using buffers kept at 4^{o}C. 25 ml columns were loaded with 1.25 ml bed volume of Ni-NTA agarose (Qiagen) and equilibrated with 2x column volumes of buffer (50 mM Tris, pH 8.0 + 200 mM NaCl + 5 mM imidazole). The cell lysate from induced cultures was passed through the columns 2x using gravity flow. The Ni-NTA agarose was then washed with 1x column volume of wash buffer A (50 mM Tris, pH 8.0 + 500 mM NaCl + 30 mM imidazole) and 0.5x column volume of wash buffer B (50 mM Tris, pH 8.0 + 500 mM NaCl + 60 mM imidazole). Finally, the eluate was collected by passing 5x bed volume of elution buffer (50 mM Tris, pH 8.0 + 500 mM NaCl + 250 mM imidazole) through the column.

In preparation for the next step of the purification process, the eluted proteins were dialyzed against buffer A (20 mM phosphate buffer; pH 7.4) at 4^{o}C. Ion exchange chromatography was then conducted using a 5 ml HiTrap Q HF column at a linear gradient from 100% Buffer A targeting 50% Buffer B (20 mM phosphate buffer + 1 M NaCl; pH 7.4). Fractions containing the purified proteins of interest were collected, analyzed with SDS-PAGE, pooled, and dialyzed against 1X PBS at 4^{o}C.

13. Cloning and purification of co-expressed his-p23 and p24

The cloning and purification schematic of his-p23 and p24 is exactly the same as described for the individual recombinant proteins. The only difference is that the PCR insert at the multiple cloning site began with the start codon for ORF23 and ended with the last codon for ORF24. There are only 12 bp separating the two ORFs. It should be noted that ORF24 was not cloned into a separate site with its own promoter and tag.

14. Inclusion body protein extraction

Overnight cultures of the clones carrying the recombinant constructs were inoculated into BHI medium and induced with IPTG (0.5 mM final concentration). Recombinant protein expression was allowed to proceed for 4 h shaking at 37^{o}C before pellets were collected via centrifugation (Sorvall SLC-6000 rotor; 7200 rpm; 30 min; 4^{o}C). The cell pellets were completely resuspended in room temperature BugBuster reagent, using 5 ml per gram of wet pellet weight. The cell suspensions were incubated for 20 min rotating at room temperature and centrifuged (Sorvall SS-34; 16,000 rpm; 20 min; 4^{o}C). The supernatants with soluble protein were saved for SDS-PAGE analysis.

The pelleted inclusion bodies were then resuspended in the same volume of BugBuster reagent. Lysozyme was added at 200 µg/ml final concentration and the mixture was vortexed and incubated at room temperature for 5 min. 6 volumes of 1:10 diluted BugBuster reagent was

added to the suspension before another vortex for 1 min. The suspension was centrifuged (Sorvall SS-34; 16,000 rpm; 15 min; 4^{o}C) and washed 3X in 1:10 diluted BugBuster. The final pelleted inclusion body fraction was resuspended in PBS and analyzed using SDS-PAGE along with the soluble protein fractions.

15. Inhibition of phage infection

Overnight cultures of *B. anthracis* ΔSterne (12 µl) were mixed with molten soft agar (0.8%; 400 µl) and overlayed onto BHI agar plates measuring 35 x 10 mm. After letting the bacterial soft agar sit for 15 min, various dilutions of the purified his-tagged phage protein stocks (PBS dilutions; 100 µl) were evenly overlaid on top. The protein overlay was incubated atop the bacterial agar for 15 min before a final overlay of Wip1 phage (~100 PFU) was evenly added. Resulting plaques were counted at 48 hrs post infection. All steps were conducted at room temperature.

16. Inhibition of phage adsorption using polyclonal antisera against his-p23

To generate polyclonal antisera against his-tagged Wip1 p23, 500 µg of the purified protein was run on an SDS-PAGE gel and excised bands were used as antigen to immunize 2 New Zealand white rabbits. Pre-immune serum

was collected before the first immunization in complete Freund's adjuvant and for the second, third, and fourth immunizations in incomplete Freund's adjuvant. Immunizations and production bleeds were collected at 3-week intervals for a total of 21 weeks.

The antisera were then tested for ability to inhibit Wip1 phage binding activity. Various dilutions of serum (in BHI media) were mixed with Wip1 phage stock (~800 PFU) and incubated in a 37ºC waterbath for 30 min. After adding 100 µl of overnight cultures of *B. anthracis* ΔSterne, the serum-phage-bacterium mixtures were incubated at room temperature for 30 min. Bacterial pellets were collected via centrifugation at 12,500 rpm for 30 seconds, washed, and resuspended in 10 mM K Phosphate buffer. Bacteria-bound phage were plated onto BHI and proceeded to form plaques overnight. The inhibition rate was measured as the percentage reduction of Wip1 PFUs as compared to a no-serum, PBS control.

17. Indirect immunofluorescence microscopy

The following protocol is a modified version of one previously described [72]. Overnight cultures of various bacterial strains were inoculated at a 1:100 dilution in BHI media and grown to mid-exponential phase (unless otherwise noted) by shaking for 3 h at 30^{o}C. The cell cultures were then pelleted by centrifugation (Eppendorf 5810 R; 4,000 rpm; 5 min; 4C), washed, and then resuspended in PBS. To fix the cells, paraformaldehyde and NaPO4, pH 7.4

were added to the suspension at final concentrations of 2.6% and 30 mM, respectively. The cells were incubated for 15 min at room temperature, followed by 30 min on ice, washed with PBS, and then attached to polylysine-coated glass cover slips. The fixed cells attached onto glass were then washed with PBS and blocked with PBS containing 1% BSA for 15 min. The cells subsequently underwent a series of 3 labeling steps: first with purified his-tagged Wip1 protein, then with anti-His mouse antibodies, and finally with anti-mouse rhodamine dye and 4',6-diamidino-2-phenylindole (DAPI) strain. Each labeling step consisted of incubating the cells with the labeling mixture for 45 min in a moist chamber and was followed by thorough washes with PBS. To reduce bleaching, the slides were mounted with 50% glycerol and 0.1% p-phenylenediamine in PBS pH 8.0. Images were captured using a Delta-Vision image restoration microscope (Applied Precision/ Olympus) equipped with CoolSnap QE cooled CCD camera (Photometrics). An Olympus 100x oil immersion objective was used in conjunction with a 1.5x optovar.

18. Pull-down assay using his-p23 and Ni-NTA

Overnight cultures of *B. anthracis* ΔSterne and *B. cereus* ATCC 4342 were inoculated in BHI media and grown to exponential phase by shaking for 3 h at 30^{o}C. After being pelleted and washed in PBS, the cells were then resuspended in PBS + 30% raffinose. PlyG lysin was added and the mixture was incubated for 1 h at 37^{o}C. The intact cell protoplasms were pelleted and

the dissociated cell wall fragments remaining in the supernatant were removed for use in the pull down assay. The following steps using Ni-NTA agarose were conducted with the same buffers and conditions as the Ni-NTA purification scheme previously outlined in this study. The Ni-NTA columns were equilibrated and loaded first with purified his-tagged viral ligand p23 and then with the cell wall supernatant. Multiple subsequent washes and elution fractions were collected, concentrated with TCA precipitation, and evaluated on SDS-PAGE gels.

19. Phage adsorption assay using protease treated cells

Overnight cultures of stationary phase *B. anthracis* ΔSterne and *B. cereus* ATCC 4342 were pelleted, washed, and resuspended in either PBS, PBS + pronase (1 mg/ml), or PBS + protease (1 mg/ml). After incubating the cells for 1 h at 37^{o}C, they were pelleted, washed, and resuspended in PBS. Treated and untreated cells were then incubated with Wip1 phage for either 5 or 20 min at 37^{o}C before spin filtration. The unbound phages in the filtrate were titered using ΔSterne and plated on BHI agar.

20. Bacterial surface carbohydrate extraction

The following procedure was conducted over the course of approximately one week with pellets frozen overnight each day. Overnight

cultures of *B. anthracis* ΔSterne and *B. cereus* ATCC 4342 were inoculated in BHI media and grown for 6 h at 30°C. This culture was then used to inoculate multiple liters of BHI media grown to stationary phase by shaking overnight at 30°C. Cells were collected via centrifugation (Sorvall SLC-6000 rotor; 7200 rpm; 30 min; 4°C) and washed multiple times with PBS before a final pellet was frozen at -80°C. Frozen cells were resuspended in cold ddH2O using 1 ml of water per 0.5 g wet weight of pellet. After lysis by passing 3X through a French Pressure Cell at 15,000 – 20,000 psi, cell walls were separated via centrifugation (Sorvall SS-34 rotor; 15,000 rpm; 30 min; 4°C). These cell wall pellets were washed for a minimum of 6X with PBS ensuring vigorous resuspension between each wash. The final pellet was resuspended again in cold ddH2O using approximately 10 ml per 1.0 g wet weight of pellet.

To dissociate cell wall-anchored proteins, this suspension was slowly added to a boiling solution of 2% SDS for roughly 15 min before cooling down at room temperature for 30 min. Boiled cell walls were then sedimented via centrifugation (Sorvall GS-3 rotor; 8,000 rpm; 40 min; 4°C) and washed at least 4X with ddH2O to remove traces of SDS. Cell wall associated carbohydrates were then separated using a hydrofluoric acid treatment. Cell wall pellets resuspended in ddH2O were frozen in a vacuum tube using a dry ice and ethanol bath before overnight lyophilization. For each 100 mg of lyophilized cell wall product, 20 ml of 48-51% hydrofluoric acid was added while stirring. This solution was first incubated at room temperature for 1 h

without a cover and subsequently incubated at 4°C overnight with a secure cover.

The next morning, the solution was centrifuged (Sorvall SS-34 rotor; 14,000 rpm; 10 min; 4°C) and the peptidoglycan-associated carbohydrates in the supernatant were saved in a polypropylene container. Each 1 ml of supernatant was treated with 5 ml of absolute ethanol and incubated at 4°C for 1 h. This solution was centrifuged (Sorvall GS-3; 8,500 rpm; 30 min; 4°C) and the resulting pellet was then washed 3X with absolute ethanol (Sorvall SS-34; 16,000 rpm; 30 min; 4°C). The final polysaccharide pellet was left uncovered at room temperature for 30 min to allow ethanol to evaporate before being frozen at -20°C. Later, the precipitate was dissolved in cold ddH2O, lyophilized, and stored at 4°C.

21. Surface carbohydrate inhibition assay

The lyopholized surface polysaccharides from hydrofluoric acid treatment were resuspended in ddH2O at a final concentration of 8 mg/ml. Various titers of Wip1 phage stock (100 µl) were incubated with aliquots of the extracted surface carbohydrates (100 µl) for 40 min in a 37°C waterbath. Carbohydrate to phage ratios ranged from 0.8 mg carbohydrate sample per 100 PFU Wip1 to 0.8 mg carbohydrate sample per 100,000 PFU Wip1. After incubation, the mixtures were titered on *B. anthracis* ΔSterne using BHI plates.

C. RESULTS

1. Wip1 morphology

Wip1 phage produced clear plaques on *B. anthracis* Sterne and ΔSterne strains. Samples of the viral particles with and without the bacterium *B. anthracis* ΔSterne were analyzed by transmission electron microscopy. Wip1 phage alone appeared as tailless, bilayer, icosahedral particles with a vertex to vertex diameter of approximately 60 nm, similar in morphology to other tectiviral phages.

Treatment with chloroform inhibited Wip1 activity, which is consistent with Wip1 possessing an inner lipid membrane (Figure 5). A control phage without a lipid membrane, W2, was not affected by chloroform treatment in its infectivity against host strain *B. cereus* ATCC 4342. Interestingly, chloroform treatment produced a 1.0×10^{-4} PFU/ml reduction in Wip1 infectivity but did not completely eliminate activity. In contrast, tectiviruses Bam35 and GIL16 are completely disrupted by chloroform treatment. However, treatment with organic solvents, such as chloroform and ether, for 30 minutes also inactivated AP50 to a survival of about 1×10^{-4} PFU/ml [40]. It is suspected that this characteristic indicates a different lipid composition from the others [73].

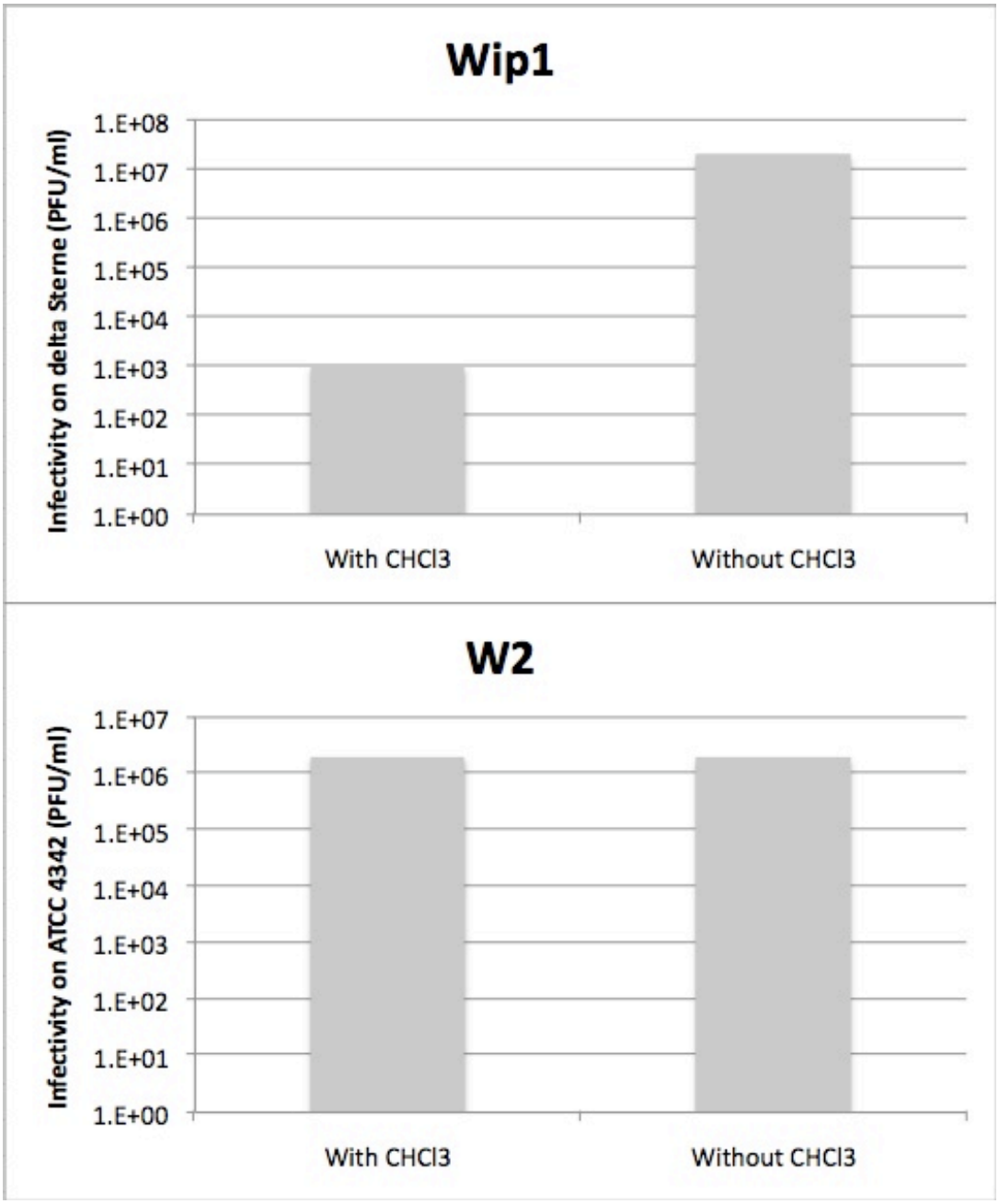

Figure 5. Effect of chloroform treatment on Wip1 and W2 infectivity

Wip1 and W2 were tested for chloroform sensitivity by incubating phage with chloroform for 15 minutes before titering on the respective host strain. Wip1 exhibited inactivation while W2, which does not contain a lipid membrane, did not.

Upon incubation with its host *B. anthracis* ΔSterne, Wip1 displayed a tube-like structure (Figure 6) that has been described in other tectiviruses including Bam35 and PRD1 [3, 22, 36]. In PRD1, interaction of protein P2 with the host receptor leads to a conformational change that results in the dissociation of the spike complex proteins from the virion [32]. This is followed by the transformation of the spherical internal membrane into a tubular channel structure for the delivery of viral DNA into the host [34, 74]. In some cases, the Wip1 tube-like structures were seen to interact in a conventional manner with the bacterial cell surface. However, interestingly, TEM images captured several Wip1 phages with tube-like structures facing away from the bacterial surface (Figure 6: B,C) instead of directly towards the host, a phenomenon not observed in other tectiviruses [75]. This could indicate that the labile vertex undergoing tubular transformation may not be the same as the vertex that initially binds the receptor. This could also be explained by reversible binding between the Wip1 tube-like structure and its host.

A.

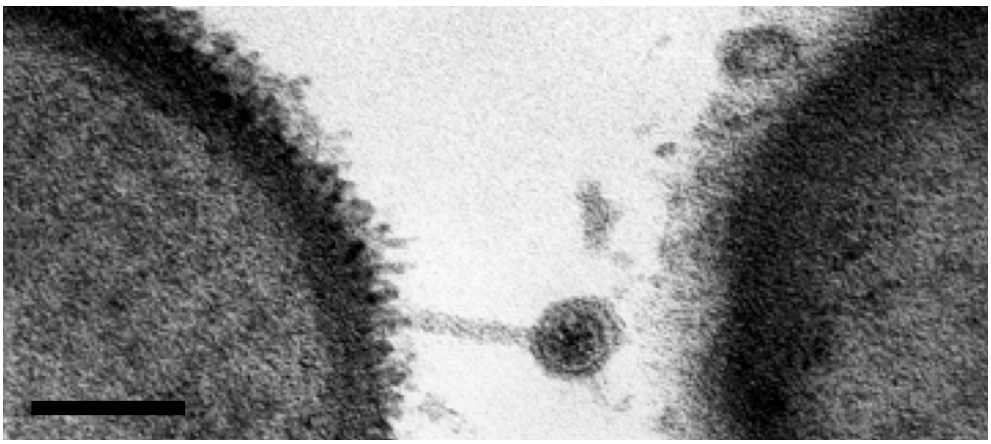

B.

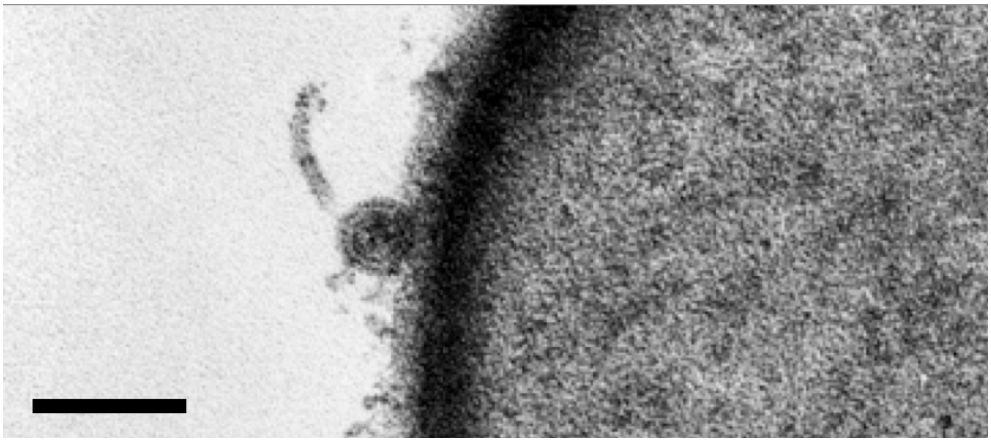

C.

Figure 6. TEM images of Wip1 upon adsorption

Wip1 was incubated with *B. anthracis* ΔSterne for 5 minutes at a MOI of 10 before being fixed for TEM imaging. Scale bar = 0.1 μ

2. Wip1 stability

Wip1 was tested for stability over time in different buffer conditions, such as BHI (brain heart infusion), PBS (phosphate buffered saline), PM2 phage buffer (20 mM Tris-HCl, pH 7.2), SM phage buffer (50 mM Tris-Cl, pH 7.0; 0.1 M NaCl; 8 mM MgSO4; 5 mM CaCl2), and Bam35 phage KP buffer (10 mM K Phosphate, pH 7.2). Results across the various buffers were similar, with Wip1 retaining infectivity fairly well in each buffer. Bam35 phage potassium phosphate (KP) buffer was selected as the standard Wip1 buffer in all subsequent experiments for consistency.

High titer stocks of filtered Wip1 phage stored in 10 mM K Phosphate buffer at 4^{o}C exhibited higher stability over time than did Bam35 stored in the same buffer. While Bam35 experienced a decay of infectivity of about 1 log per 12 days [37], Wip1 experienced an approximately 1 log decrease in infectivity per 60 days. Remarkably, Wip1 also retained its infectivity after exposure to UV for up to 5 minutes and vigorous vortexing for up to 2 minutes (data not shown). Experiments in this study that required serial dilutions of Wip1 phage utilized vortexing for up to 30 seconds as a technique for rapid and thorough mixing.

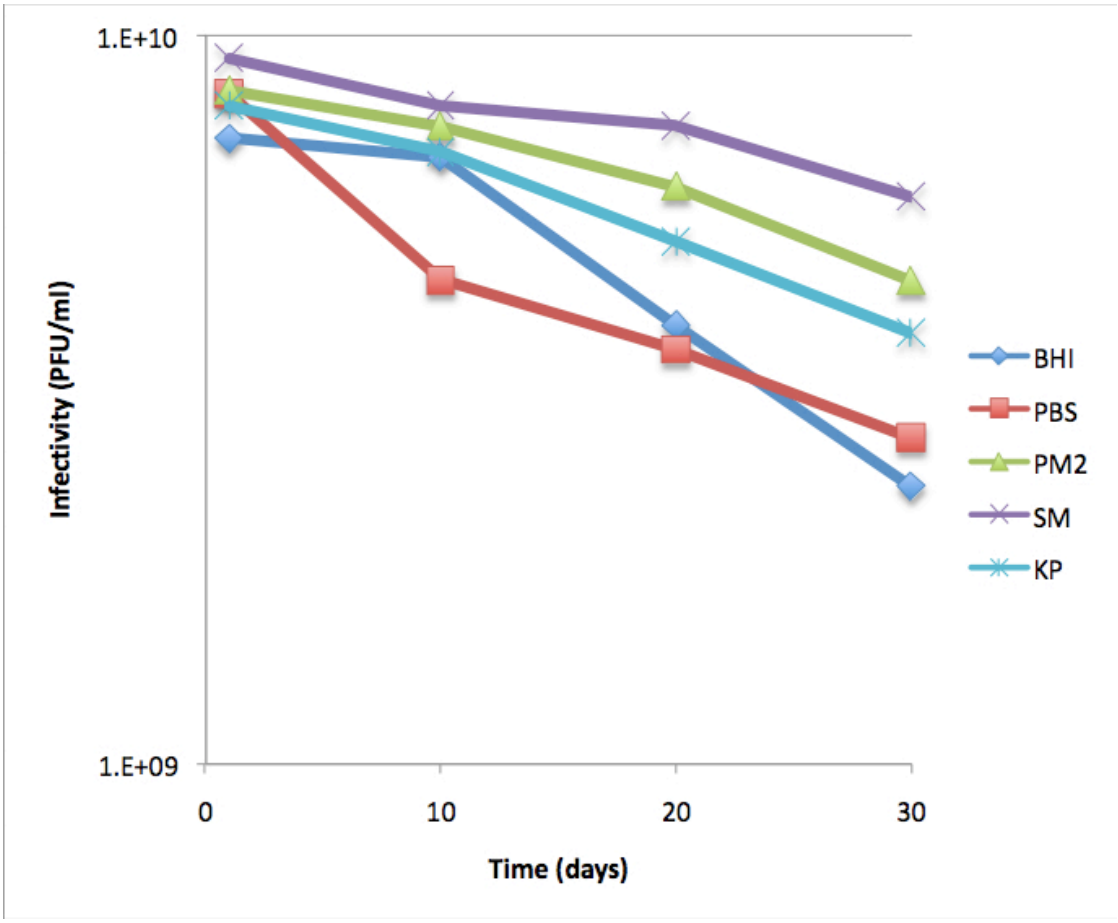

Figure 7. Wip1 stability in various buffers

Wip1 was tested for infectivity over time in storage at 4°C in various buffers: BHI (brain heart infusion broth), PBS (137 mM NaCl; 2.7 mM KCl; 4.3 mM Na2HPO4; 1.47 mM KH2PO4; pH 7.4), PM2 phage buffer (20 mM Tris-HCl, pH 7.2), SM phage buffer (50 mM Tris-Cl, pH 7.0; 0.1 M NaCl; 8 mM MgSO4; 5 mM CaCl2), and KP buffer (10 mM K Phosphate, pH 7.2).

Wip1 lost infectivity during phage purification schemes that involved either CsCl or sucrose gradients. Stepwise gradients using CsCl produced two major bands, one at 1.3 g/ml and the second between 1.2 and 1.25 g/ml (Figure 8). Continuous gradients using 20 – 70% sucrose normally produced one major band between 60 – 70%, although one particular sucrose gradient spin produced multiple bands (Figure 8). All bands were extracted by either needle puncture or by fractionation and tested for phage activity. Unfortunately, the particles recovered from the bands exhibited infectivity of only 1×10^2 PFU/ml, a significant decrease from the original 1×10^{10} PFU/ml stock used for the gradients. No infectivity was detected in any other fractions.

Similarly, CsCl gradients were also found to significantly decrease Bam35 infectivity [37]. The high ionic strength environment was thought to cause coat protein dissociation from the virion. Due to the observed inactivation of phage, CsCl and sucrose gradient purification schemes were abandoned. All subsequent experiments performed with Wip1 phage used filtered high titer stocks in a solution of BHI/ 10 mM potassium phosphate, pH 7.2.

A.

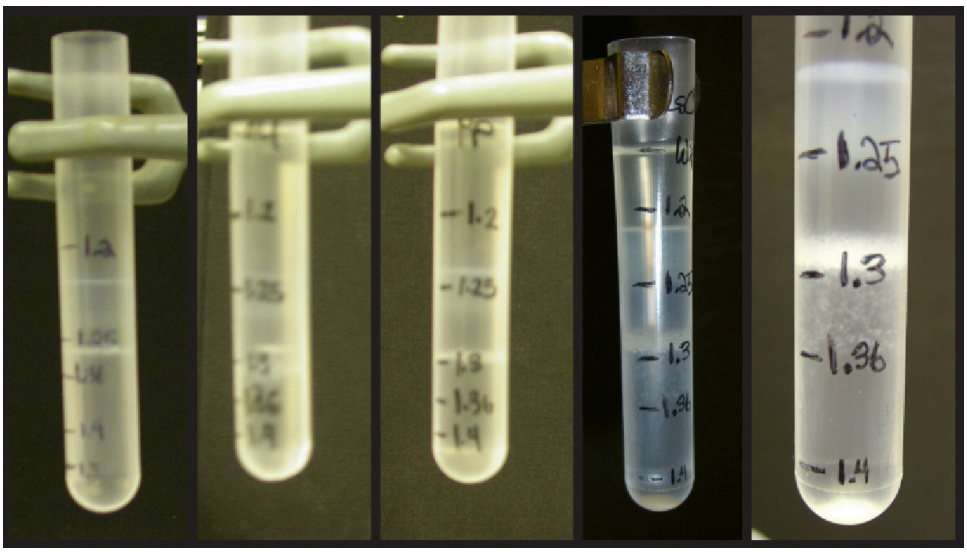

B.

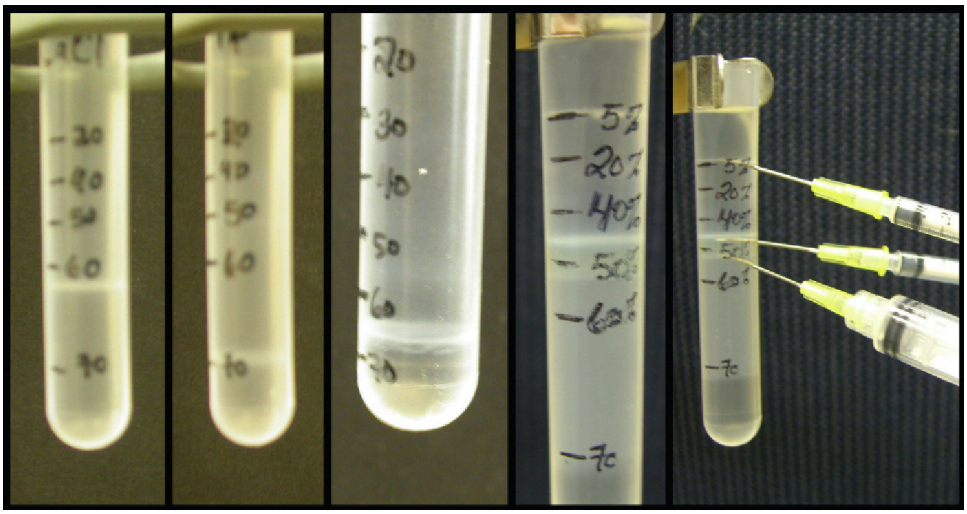

Figure 8. Bands resulting from CsCl and sucrose gradients with Wip1

A. CsCl gradients

B. Sucrose gradients

CsCl and sucrose gradient purification of Wip1 phage produced visible bands that were extracted. However, particles recovered from the bands exhibited a 1 x 10^{-8} PFU/ml loss of infectivity from the original titer. None of the other gradient fractions exhibited phage activity

3. Wip1 adsorption is specific to *B. anthracis*

Previous studies determined that Wip1 infectivity is more specific to *B. anthracis* than is the standard diagnostic tool Wγ phage [1]. This host range study was expanded to include both infectivity and adsorption of Wip1 virions to various strains. Infectivity was measured by titering phage directly against test strains on agar plates. Adsorption was assayed by incubating Wip1 with test strains for 20 minutes, separating bacterium-bound phage via centrifugation and filtration, and then titering the unbound phage in the supernatant on *B. anthracis* ΔSterne. The adsorption rate was calculated as the percentage of bound Wip1 phage (# total phage – # unbound phage) out of the total phage count (as determined by a buffer only control).

The narrow range of adsorption showed that Wip1 binding exhibited a high specificity to *B. anthracis* that corresponded to its narrow infectivity host range (Table 2). Wip1 exhibits high infectivity of 6×10^9 and a 100% adsorption rate on host strain *B. anthracis* ΔSterne. Similarly, Wip1 exhibits infectivity of 3×10^7 and a 94% adsorption rate on *B. cereus* CDC32805. On the other hand, Wip1 does not infect *B. cereus* ATCC 4342 and correspondingly does not adsorb to it. These observations further support the model of Wip1 tropism being mediated by the receptor binding proteins on its surface.

Table 2. Wip1 infectivity and adsorption range

Various bacterial strains were tested for Wip1 infectivity and adsorption. The lower limit of detection of infectivity is indicated by "< 10", while the lower limit of detection of adsorption is indicated by "< 5". The Wip1 host range is highly specific for *B. anthracis* in terms of both infectivity and adsorption.

	Infectivity (PFU/ml of phage stock)		**Adsorption (%)**
Strain	Wgamma	Wip1	Wip1
Bacillus anthracis			
delta Sterne	3.0E+09	6.0E+09	100
Bacillus cereus			
ATCC 4342	1.0E+05	< 10	< 5
CDC32805	4.0E+07	3.0E+07	94
CDC13100	< 10	< 10	< 5
CDC13140	< 10	< 10	< 5
ATCC 10987	< 10	< 10	< 5
NRL 569	< 10	< 10	< 5
ATCC 14579	< 10	< 10	< 5
ATCC 13472	< 10	< 10	< 5
ATCC 11980	< 10	< 10	< 5
RTS 100	< 10	< 10	< 5
Bacillus thuringiensis			
HD1	< 10	< 10	< 5
HD73	< 10	< 10	< 5
Bacillus subtilis SL4	< 10	< 10	< 5
Bacillus pumilis SL4680	< 10	< 10	< 5
Sporosarcina ureae	< 10	< 10	< 5
Bacillus megaterium WH32	< 10	< 10	< 5
Brevibacillus laterosporus	< 10	< 10	< 5

Wip1 adsorption kinetics was studied by assaying the amount of bound phage at various time points. As expected, *B. cereus* ATCC 4342 bound < 5% of Wip1 phage, the lower limit of detection of adsorption. On the other hand, stationary phase *B. anthracis* ΔSterne bound approximately 80% of virus particles during the first minute after phage adsorption and had adsorbed 99% after 10 minutes (Figure 9). Bam35 experienced similar adsorption kinetics with various *B. thuringiensis* strains. Strain 4I1 bound ~65% of phage in the first minute and ~90% after 10 minutes, while strain HER1410 was found to bind ~80% of virions in the first 20 seconds and 96% by 5 minutes [39]. Both Wip1 and Bam35 adsorb very rapidly to their respective host cell surfaces.

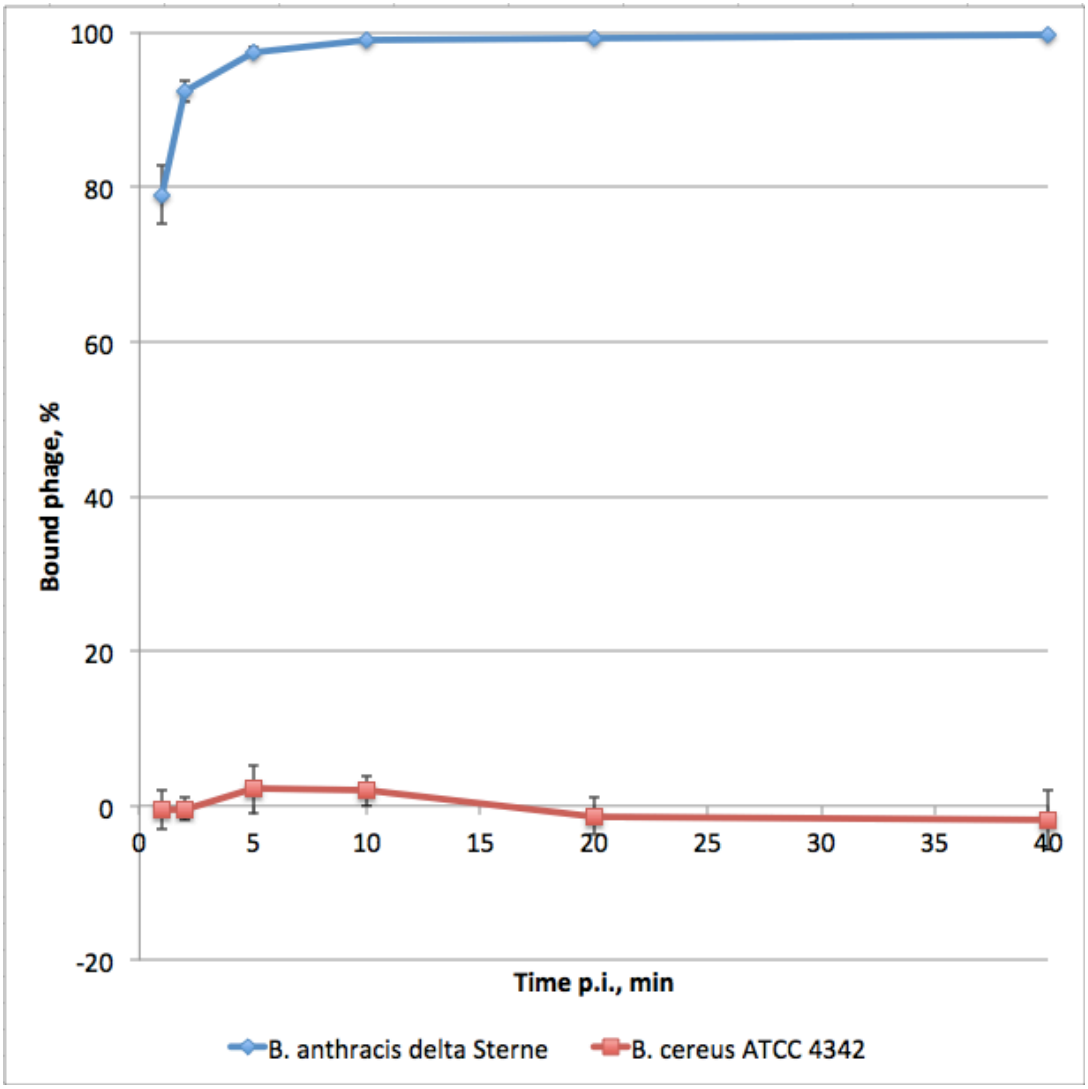

Figure 9. Wip1 adsorption kinetics

Wip1 was incubated with either *B. anthracis* ΔSterne or *B. cereus* ATCC 4342 for various lengths of time. Unbound phages were separated via centrifugation and filtration before being titered on ΔSterne. The adsorption rate was calculated as the percentage of bound phage (total – unbound) out of total phage. Bars represent standard errors of 6 experiments at MOIs from 1e-4 to 10.

4. Wip1 DNA analysis

DNA was isolated from Wip1 phage by first denaturing the viral coat proteins using protease K and SDS. After the denatured proteins were removed by extraction with organic solvents phenol and chloroform, the DNA was precipitated with ethanol and stored in buffer.

Based on DNA analysis, the Wip1 genome was determined to be a linear molecule of dsDNA. Pulse field gel electrophoresis of purified Wip1 DNA revealed a strong band estimated to be approximately 15 kbp (Figure 10). This length is consistent with that of other tectiviruses, including Bam35c (14,935 kb) and PRD1 (14,925 kb). The double stranded nature of the DNA was indicated by both band migration according to its sequenced length and ethidium bromide (EtBr) staining. EtBr is a fluorescent tag that preferentially intercalates double stranded structures of nucleic acids. Although it is possible for EtBr to stain ssDNA, the signal is very weak. Serially diluted samples of Wip1 DNA exhibited efficient EtBr staining indicative of dsDNA.

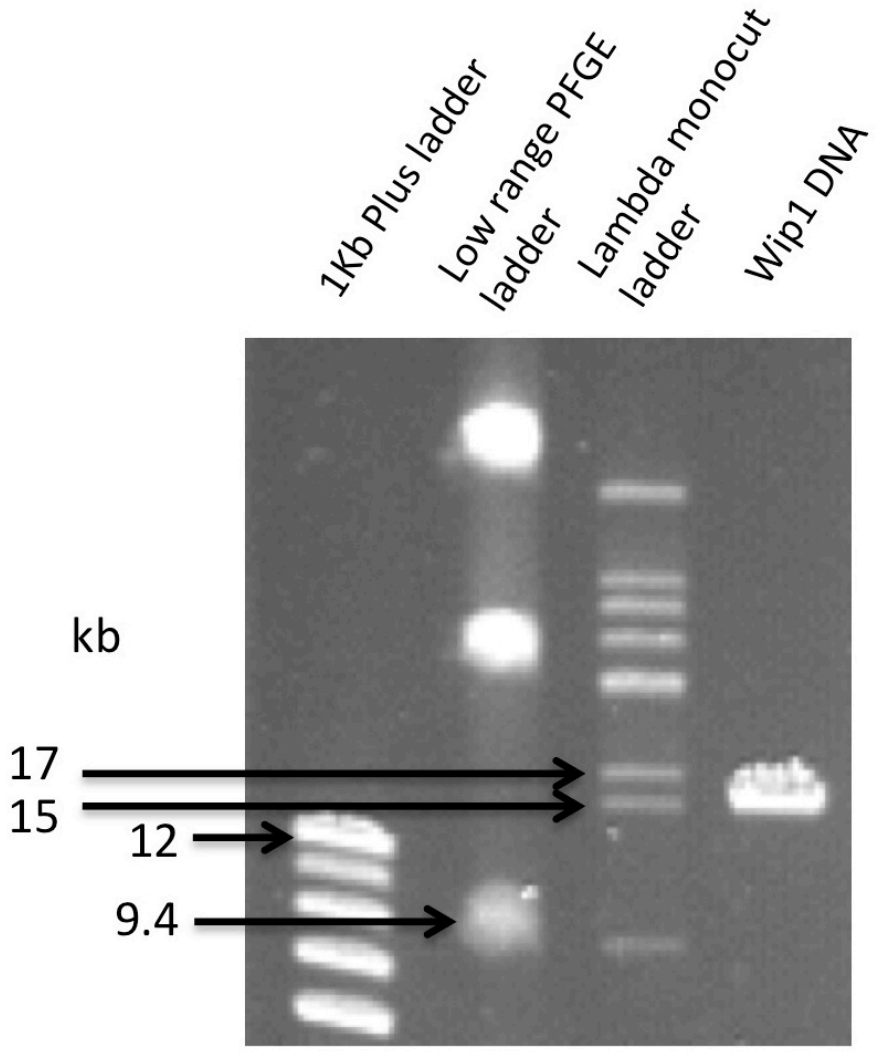

Figure 10. PFGE of extracted Wip1 DNA

Pulse field gel electrophoresis migration of extracted Wip1 DNA was analyzed along side 1Kb Plus, Low range PFGE, and Lambda Monocut ladders.

The extracted genomic DNA was tested for the presence of covalently linked terminal proteins. DNA isolated from PRD1 and Bam35 was attached to terminal proteins and could not properly enter an agarose gel, but protease treatment allowed proper DNA migration [37]. In contrast, we observed similar migration between Wip1 DNA treated with and without protease (Figure 11). This observation suggested that, unlike the PRD1 and Bam35 genomes, Wip1 DNA is not associated with proteins.

However, the DNA extraction method was later re-evaluated for potential removal of DNA-associated proteins even before the protease treatment assay was conducted. It was originally thought that the Wip1 inner membrane would protect its DNA from exposure to the protease step used to remove coat proteins before phenol inactivation. But dissociation of the PRD1 spike complex protein P2 has been shown to promote tubular transformation and DNA delivery [3]. It is possible that protease K digestion of the viral capsid also leads to DNA release, which would expose the genome to protease during the original DNA extraction. Due to this possibility, the protease treatment assay was deemed to be inconclusive.

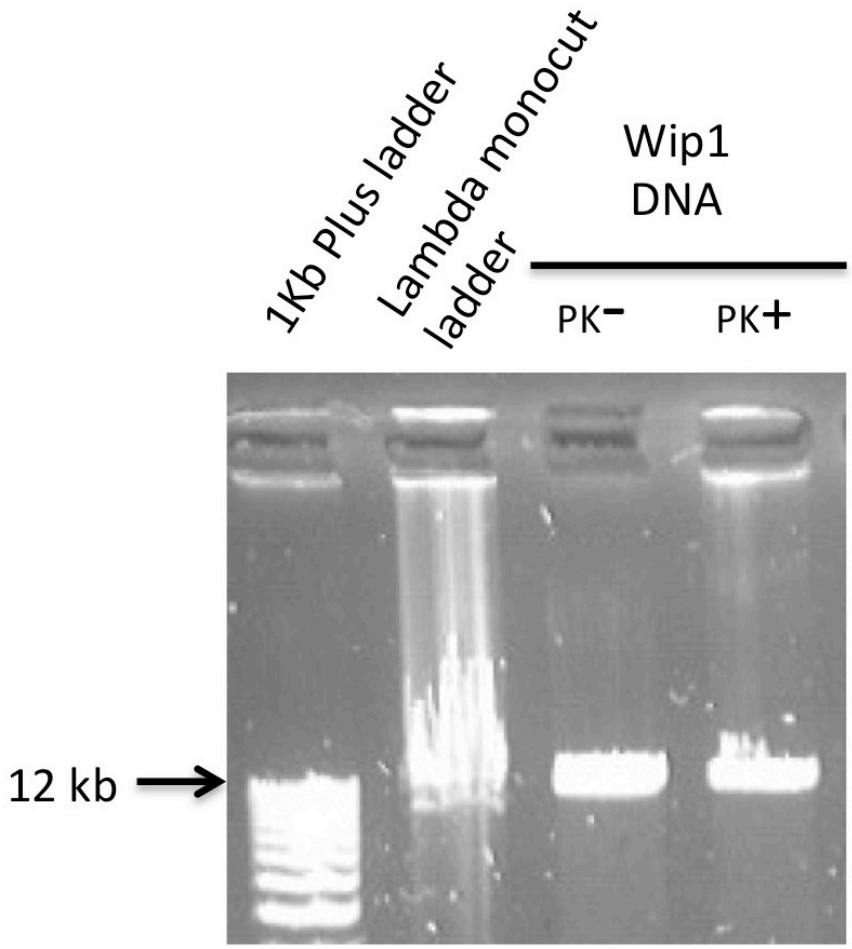

Figure 11. Gel of Wip1 DNA with and without protease treatment

Extracted Wip1 DNA was treated with and without protease K before subsequent purification using phenol/ chloroform extractions and ethanol precipitation. Migration of the resulting DNA samples was analyzed with agarose gel electrophoresis.

5. Wip1 genome analysis

Linker-mediated PCR amplification and shot-gun based sequencing determined the Wip1 genome length to measure 14,319 bp. The closest reported virus in the NCBI database in terms of genome size is AP50 with 14,398 bp. The average guanine-cytosine (GC) content of Wip1 is 36.9%, which is lower than that reported of other tectiviruses such as Bam35c (39.7%) and PRD1 (48.1%) [37]. We noted that the Wip1 genome GC content at both extremities is lower than the percentage observed in the central section of the genome. The first and last genes, ORF1 and ORF27, have GC contents of 29.5% and 29.7%, respectively. In contrast, ORF18 and OPF19, located at the genome center, have GC contents of 43.1% and 44.8%, respectively (Table 3).

Detailed analysis of the Wip1 sequence revealed the existence of 27 putative open reading frames (ORFs), as listed in Table 3. The tightly organized genome with few noncoding regions, small intergenic spaces, and some overlapping ORFs is characteristic of its family *Tectiviridae*. Many of the predicted genes are remarkably short, also similar to other tectiviruses. PRD1 has been shown to code for a protein as short as 42 residues (protein P20). In comparison, the shortest predicted Wip1 genes are ORF1 and ORF11, each with 47 predicted protein residues

Table 3. Comparative analysis of predicted Wip1 ORFs with AP50, GIL16c, and Bam35c ORFs

Wip1 ORF	No. of residues (genome coordinates)	Strand	G+C content (%)	Identity (%)			ORF (no. of residues)			PRD1 protein (no. of residues)	Postulated function
				AP50	GIL16c	Bam35c	AP50	GIL16c	Bam35c		
1	47 (396-569)	+	29.5								
2	196 (598-1188)	+	30.7								Transcription factor
3	112 (1219-1557)	+	25.7								LexA-type repressor
4	91 (1690-1965)	+	25.7								
5	67 (1958-2161)	+	27.9	55.1			10 (57)				
6	116 (2121-2471)	+	43.9	69.6	68.6	55.3	11 (114)	9 (125)	10 (145)	P6 (166)	DNA packaging/ unique vertex
7	236 (2309-3019)	+	46.8	78.4	39.3	43.9	12 (235)	10 (248)	11 (252)	P10 (203)	Assembly
8	83 (2865-3116)	+	46.4	94.0	53.2	53.2	13 (83)	11 (80)	12 (80)		
9	212 (3125-3763)	+	42.4	93.9	59.9	63.7	14 (212)	13 (212)	14 (212)	P9 (227)	DNA packaging ATPase
10	54 (3760-3924)	+	36.4	89.1	60.9	60.9	15 (46)	14 (46)	15 (46)		
11	47 (3938-4081)	+	33.6	80.9	48.8	48.8	16 (49)	16 (46)	16 (46)	P20 (42)	DNA packaging/ unique vertex
12	353 (4081-5142)	+	40.7	83.8	63.0	63.8	17 (354)	18 (356)	18 (356)	P3 (395)	Major capsid protein
13	74 (5191-5415)	+	38.2	78.4	35.7	34.3	18 (74)	19 (76)	19 (76)	P22 (47)	DNA packaging/ unique vertex
14	59 (5421-5600)	+	32.8	26.5	41.3	55.8	19 (56)	20 (52)	20 (68)		
15	157 (5677-6150)	+	38.8	86.6	50.7	52.0	20 (157)	22 (143)	21 (143)		
16	61 (6138-6323)	+	36.0	79.3	60.7	60.7	21 (58)	23 (58)	22 (58)		
17	48 (6323-6469)	+	36.1	77.1	54.2	54.2	22 (48)	24 (48)	23 (48)		
18	91 (6482-6757)	+	43.1	82.4	35.0	32.5	23 (91)	25 (91)	24 (91)	P30 (84)	Minor capsid protein
19	213 (6761-7402)	+	44.8	85.1	41.7	41.7	24 (210)	26 (204)	25 (204)	P11 (207)	DNA delivery
20	218 (7402-8058)	+	44.1	91.7	65.7	64.8	25 (218)	27 (250)	26 (250)	P7 (265)	Lysin
21	175 (8055-8582)	+	46.4	84.6	61.4	62.6	26 (175)	28 (170)	27 (170)		
22	291 (8593-9468)	+	44.7	84.0	42.9	51.3	27 (304)	29 (297)	28 (304)	P5 (340)	Trimeric spike protein
23	117 (9472-9825)	+	39.8								
24	118 (9838-10194)	+	36.7	50.8			29 (118)				
25	48 (10196-10342)	+	33.3	71.7			30 (49)				
26	213 (10344-10985)	+	42.3								Lysin
27	898 (11342-14038)	-	29.7								DNA polymerase

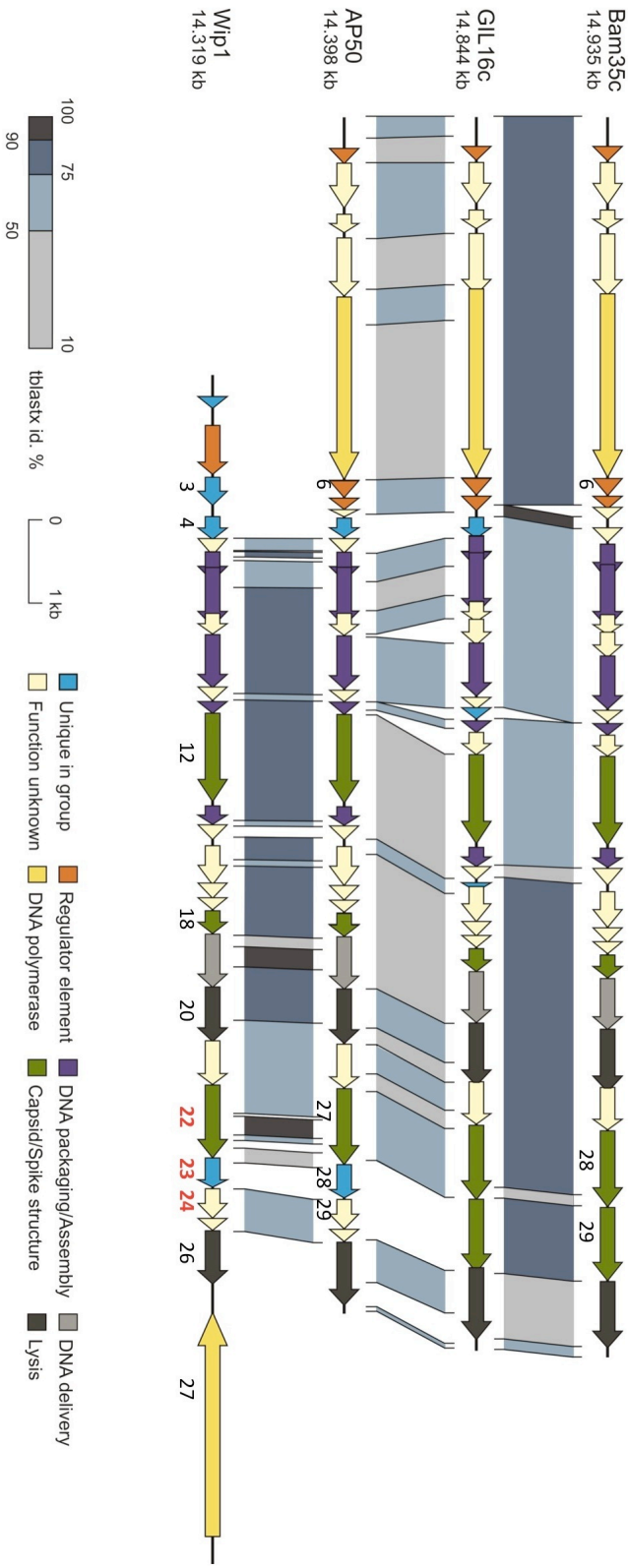

Figure 12. Map of Wip1 genome and tectiviral genome analysis

Based on BLAST analysis and tectiviral genome organization, 14 out of 27 ORFs were designated putative functions. Wip1 encodes two different lysins, ORF20 and ORF26, which are predicted to be a muramidase and an L-alanyl-D-glutamate peptidase, respectively. Interestingly, the N-terminal half of ORF20 contains a conserved FlgJ domain. FlgJ is a *Salmonella enterica* flagellar protein with peptidoglycan hydrolase activity that digests through the peptidoglycan layer to facilitate rod penetration. BLAST analysis did not identify any conserved domains for ORF26, but did indicate homology to peptidases from *B. cereus* and *Listeria*.

While Wip1 exhibits some sequence similarities to gram-positive infecting tectiviruses Bam35c and Gil16c, it is most closely related to AP50. Wip1 and AP50 both exhibit very narrow host ranges highly specific to *B. anthracis* [41]. The genome of Wip1 from ORF4 through ORF26 is strikingly similar to the section of AP50 from ORF9 through ORF31 in ORF size, sequence, and organization (Figure 12). Among the 27 total putative Wip1 ORFs, 20 share sequence identity of at least 50% to other tectiviral proteins and 15 share high sequence identity of at least 75% to AP50 proteins.

The most remarkable distinction of the Wip1 genome is the placement of the putative DNA polymerase, ORF27, at the 3' end of the genome on the negative strand. All other tectiviral DNA polymerases are encoded in the first 5000 base pairs of their genomes on the positive strand. In fact, Wip1 ORF27 is the only predicted gene found on the negative strand of any gram-positive infecting tectivirus. While the putative ExoII, S/TLx2h, Kx2h, and ExoIII motifs

of the 3'-5' exonuclease domain were identified, the unusual sequence lacked some of the more highly conserved motifs such as motif C or a clear ExoI motif. Furthermore, the unusual Wip1 ORF27 gene product does not share any significant homology with any other proteins in the NCBI database.

Another notable section of the genome involves the regulatory elements located at the beginning of the sequence. Wip1 ORF3 was predicted to be a LexA-type repressor based on BLAST homology. Despite its lack of sequence similarity to tectiviral sequences, ORF3 surprisingly aligned with the genomic position of Bam35 gp6, which is a LexA-type activator of late gene transcription. BLAST analysis also suggested that ORF2 is involved in gene regulation, which is particularly interesting since a LexA-type regulator immediately follows it. Additionally, if the DNA polymerase is indeed regulated by the phage itself, it would involve a regulator encoded at the beginning of the genome acting upon the opposite extremity, a rare phenomenon in phages. It should be noted that SOS-induction experiments using UV stimulation did not induce lysogenic Wip1 virion production.

Yet another particularly intriguing region of the genome includes Wip1 ORF22, ORF23, and ORF24. Wip1 ORF22 is predicted to be a putative spike complex protein as it shares 51.3% sequence identity with Bam35 gp28, a homolog for PRD1 trimeric spike protein P5. Bam35 gp28 is followed by gp29, a 293 amino acid protein that also resides on the phage surface. If Wip1 and AP50 genomic organization both align with that of Bam35c, then a putative spike complex protein should follow. Interestingly, in Wip1 and AP50, the

genes downstream the P5 homolog are located in a highly variable region and do not share sequence identity with any Bam35 ORFs. Despite the lack of homology, we predicted that Wip1 gene products 23 and 24 (totaling 235 amino acids together) were putative spike complex proteins based on their strikingly similar gene cassette alignment both upstream and downstream of this region. Finally, we were intrigued by the observation that while Wip1 ORF24 shares 51% sequence identity with AP50 ORF29, Wip1 ORF23 is a unique gene that does not share sequence homology to any other known genes, tectiviral or otherwise.

6. Wip1 p23 and p24 form a stable complex

Genomic analysis predicted three Wip1 proteins, p22, p23, and p24 (indicated in red in Figure 12) to be possible candidates for the Wip1 spike complex. We developed expression and purification schemes for the his-tagged constructs of all three viral proteins. However, the separately expressed his-p23 and his-p24 constructs resulted in extremely low yields of soluble protein due to the formation of inclusion bodies (Figure 13). Curiously, when his-p23 and p24 were co-expressed together, significantly higher yields of soluble protein were generated, suggesting that his-p23 and p24 assist each other in proper folding when co-expressed.

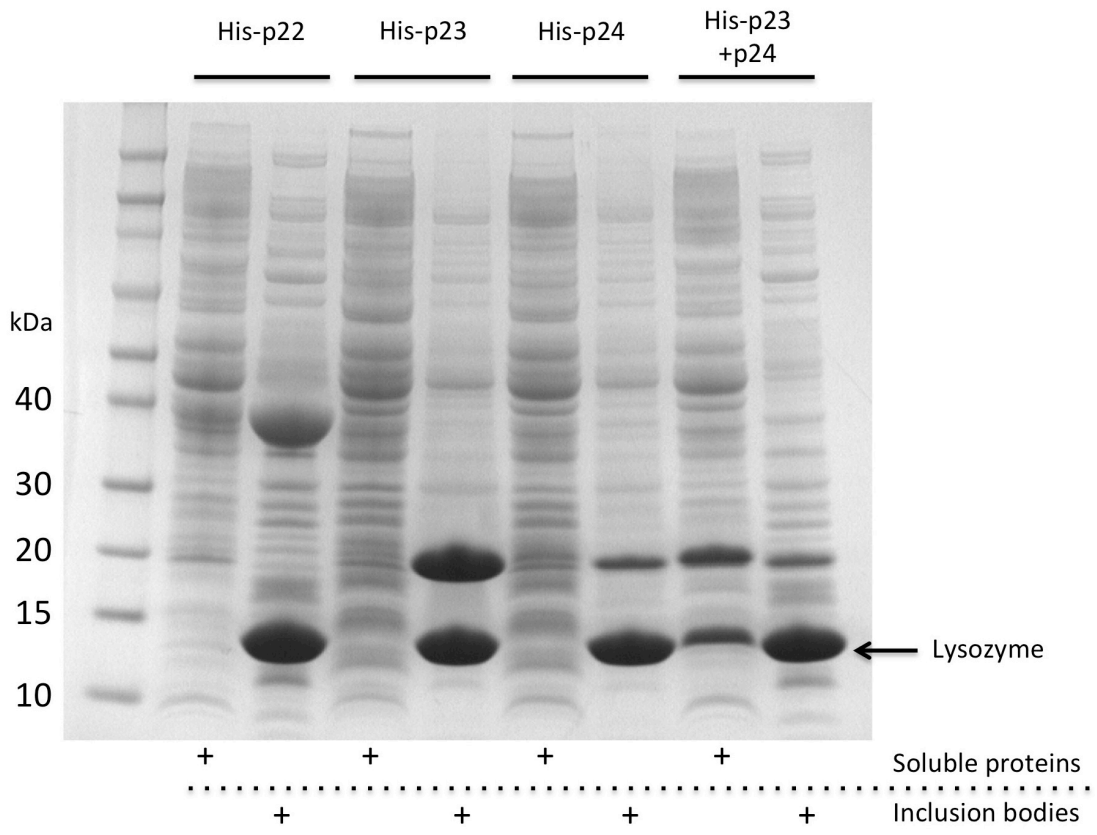

Figure 13. SDS-PAGE of soluble and insoluble recombinant protein fractions

Recombinant his-tagged constructs of viral proteins were built and expressed using methods described. Induced cell cultures underwent treatments to extract both soluble proteins and insoluble proteins from inclusion bodies (using lysozyme, 14.7 kDa). Major bands for his-p23 (18 kDa) and his-p24 (18.8 kDa) are revealed in the inclusion body extractions for each separate construct. In contrast, major bands for his-p23 (18 kDa) and p24 (13.6 kDa) are visible in the soluble fraction for the his-p23 + p24 co-expression construct.

Subsequent recombinant protein purification steps also revealed his-p23 and p24 interactions. Nickel-nitrilotriacetic acid (Ni-NTA) resins are used for rapid one-step purification of proteins containing a His-tag by preferentially binding to histidine residues. After co-expressed his-p23 and p24 proteins were processed through a stringently washed Ni-NTA column, both were eluted together despite the fact that p24 was not his-tagged (Figure 14).

In a second purification step, the Ni-NTA elution was processed through an ion exchange column that separates molecules based on their charge. Distinct peaks were observed and analyzed by SDS-PAGE, revealing unique protein populations in each peak. This indicates that ion exchange purification was successful in separating proteins and protein complexes of different charges. Again, both proteins were observed together in the same ion chromatography fractions despite the fact that his-p23 and p24 exhibit drastically different pIs of 8.4 and 4.9, respectively (Figure 14). The observation that neither purification scheme separated the two proteins strongly suggests that they form a stable complex.

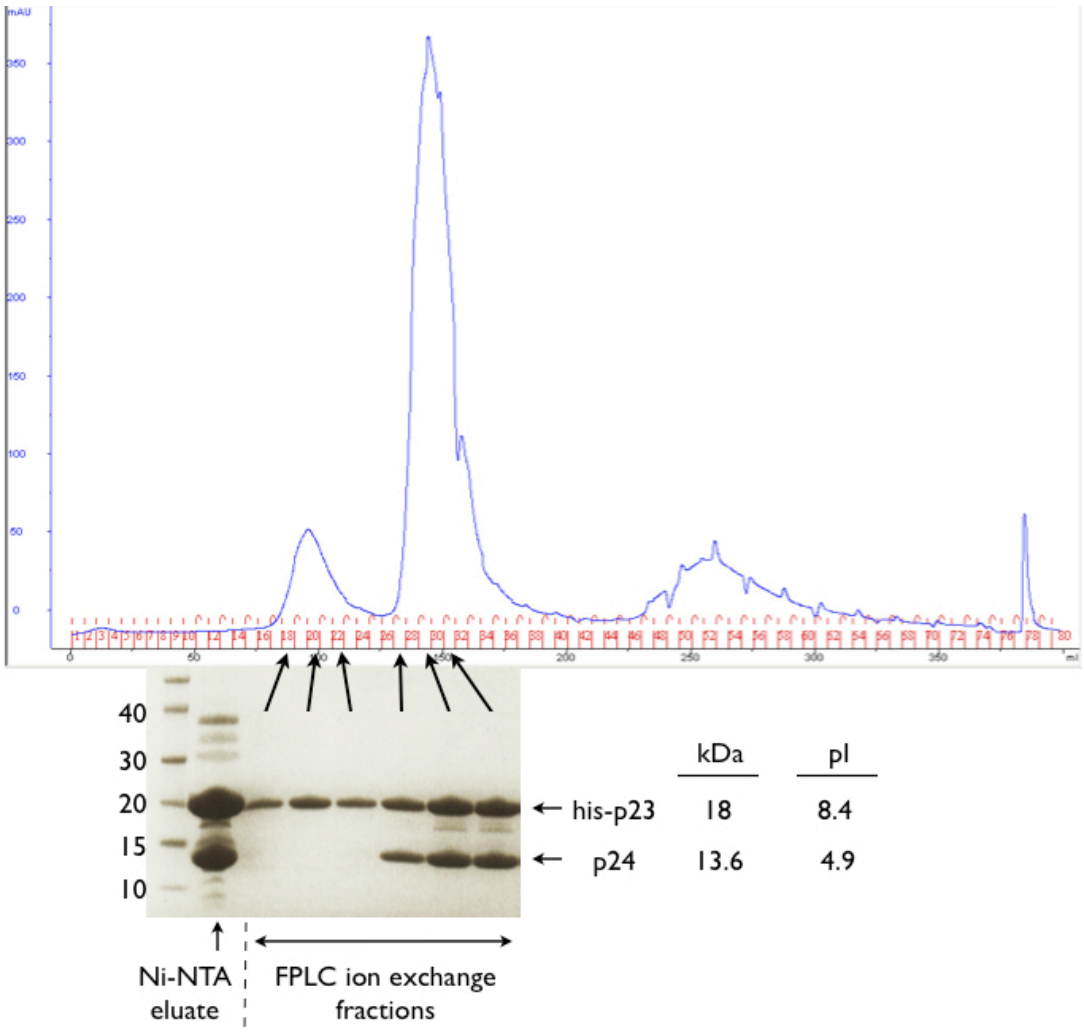

Figure 14. Ion chromatogram and SDS-PAGE of select fractions

The Ni-NTA eluate containing both his-p23 and p24 (Lane 1) was further purified by charge using ion exchange chromatography. The distinct peaks were evaluated with SDS-PAGE, which revealed the presence of his-p23 alone in Peak 1 and the presence of his-p23 and p24 together in Peak 2.

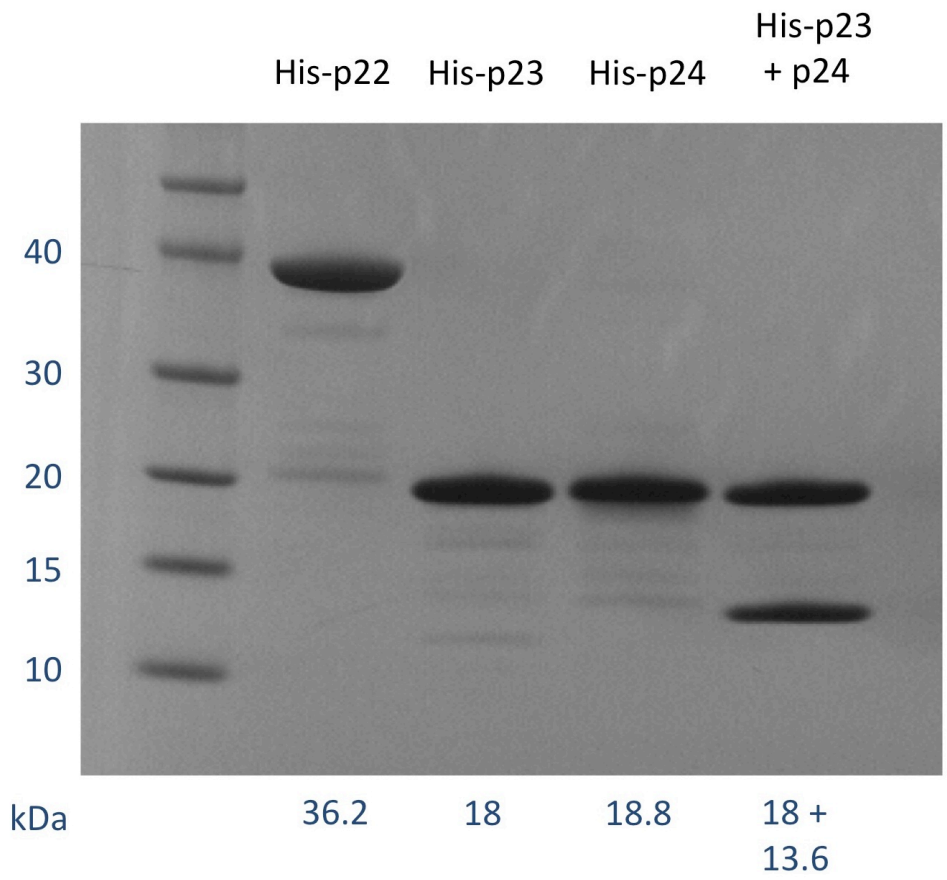

Figure 15. SDS-PAGE of final stocks of purified recombinant Wip1 proteins

Following expression and purification methods as described, the recombinant his-tagged Wip1 proteins were then measured using standard BSA assays. Protein solutions were diluted to concentrations of 250 µg/ml for single protein samples (his-p22; his-p23; his-p24) and 500 µg/ml for co-expressed protein samples (his-p23 + p24). SDS-PAGE analysis of these protein samples revealed purification to near homogeneity. The samples shown here are the exact samples used in the following protein overlay-based inhibition assays.

7. Wip1 p23 is a receptor-binding protein

The purified recombinant proteins (Figure 15) were measured by standard Bovine Serum Albumin (BSA) immunoenzymetric assays. Protein stocks were diluted to concentrations of 250 µg/ml for single protein samples (his-p22; his-p23; his-p24). The co-expressed protein complex sample (his-p23 + p24) was diluted to 500 µg/ml to account for the presence of two different proteins. These recombinant protein stocks were then used in a Wip1 activity inhibition assay, which consisted of overlaying the viral proteins on top of *B. anthracis* ΔSterne growing in soft agar plates before adding a final overlay of infectious Wip1 phage (Figure 16). The rate of infectivity inhibition was calculated as the percentage of inactivated phage (# total original phage – # infectious phage titered after incubation with recombinant protein) out of total phage (as determined by a buffer only control).

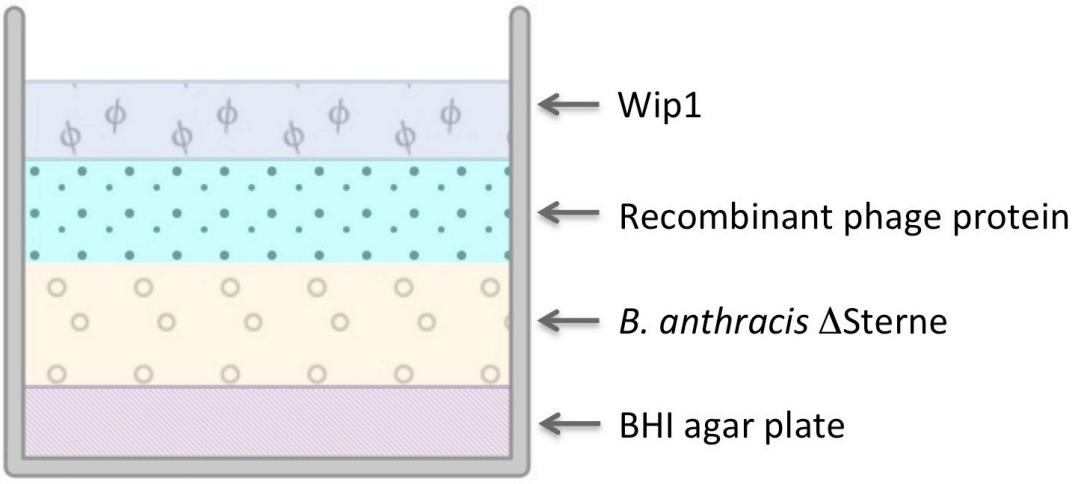

Figure 16. Schematic of a Wip1 inhibition assay using recombinant Wip1 proteins

His-p23 was shown to competitively inhibit Wip1 infectivity up to 100% in a dose-dependent manner while his-p22 and his-p24 had no effect on phage infectivity (Figures 17 and 18). This finding suggests that Wip1 p23 is a receptor-binding protein. The addition of his-p23 would occupy the available receptors on the host surface and prevent other ligands such as Wip1 phage from binding. Interestingly, the his-23 plus p24 complex exhibited even higher inhibition levels than his-p23 alone, a finding that may be explained by either increased protein stability or enhanced activity of the receptor binding complex.

The possibility that recombinant his-p22 and his-p24 may not possess their full biological activity because of the linked histidine should be noted. However, issues for his-p24 concerning potential misfolding or activity interference caused by a histidine tag are partially addressed by the properly folded and non-his-tagged p24 co-expressed with the his-p23 + p24 complex.

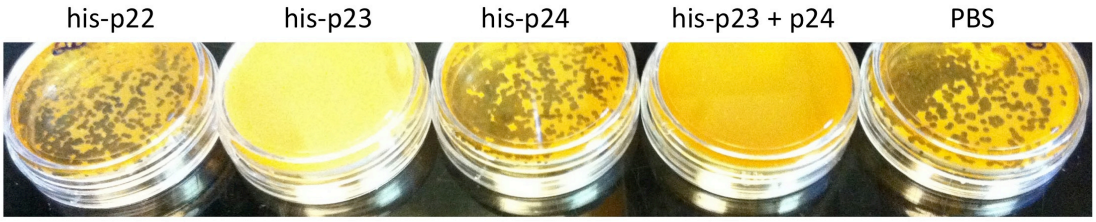

Figure 17. Photograph of Wip1 inhibition assay results

Results of the Wip1 inhibition assay using recombinant viral proteins at a concentration of 125 µg/ml per protein.

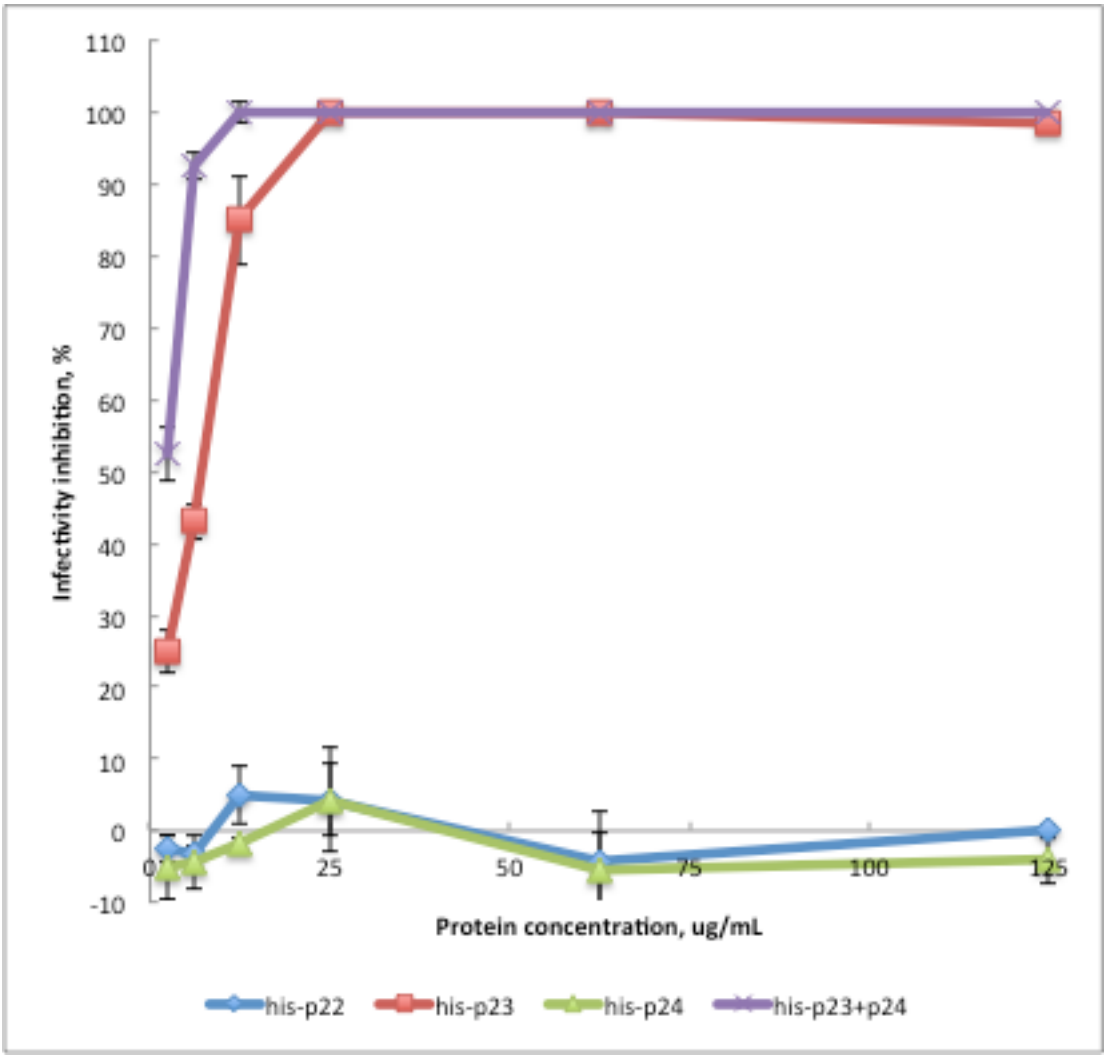

Figure 18. Wip1 inhibition of infectivity by recombinant Wip1 proteins

Wip1 phage was assayed for inactivation by recombinant viral proteins at various concentrations. Protein concentrations are indicated per protein. His-p23 (red) and the his-p23 + p24 complex (purple) inactivated Wip1 infectivity by up to 100% in a dose-dependent manner. His-p22 (blue) and his-p24 (green) did not affect phage activity. Bars represent standard error for a minimum of 3 experiments.

In a second Wip1 inhibition assay, we generated rabbit polyclonal antisera against Wip1 his-p23. The resulting anti-his-p23 antibodies were tested for neutralization of phage activity. Various dilutions of antibody serum were pre-incubated with Wip1 phage before adding *B. anthracis* ΔSterne bacteria to the mixture. After centrifugation pelleted the bacterium-bound phage, any unbound or antibody-bound phage remaining in the supernatant was removed. The pelleted cells were plated to reveal the titer of bacterium-bound phage. Adsorption inhibition was calculated as the percentage of un-adsorbed phage (# total phage - # bacterium-bound phage) out of total phage (as determined by a buffer only control).

The anti-his-p23 antibodies reduced Wip1 adsorption by up to 90% in a dose-dependent manner. Pre-bleed serum did not have an effect on Wip1 activity (Figure 19). This suggests that Wip1 p23 protein resides on the phage surface and is consistent with the finding that it is a receptor binding molecule. Anti-his-p23 antibodies would bind to p23 on the surface of Wip1 virions, preventing the phages from binding to and infecting its host.

It should be noted, however, that the neutralizing effect of anti-his-p23 serum on Wip1 activity was much weaker compared to that of anti-gp28 or anti-gp29 serum on Bam35 activity. At a mere 20x dilution, anti-his-p23 antibody inactivation measured below 20% (Figure 19). In contrast, anti-gp28 and anti-29 antibodies did not demonstrate phage inactivation rates below 20% until they reached dilutions of 5,000x and 100,000x, respectively [39].

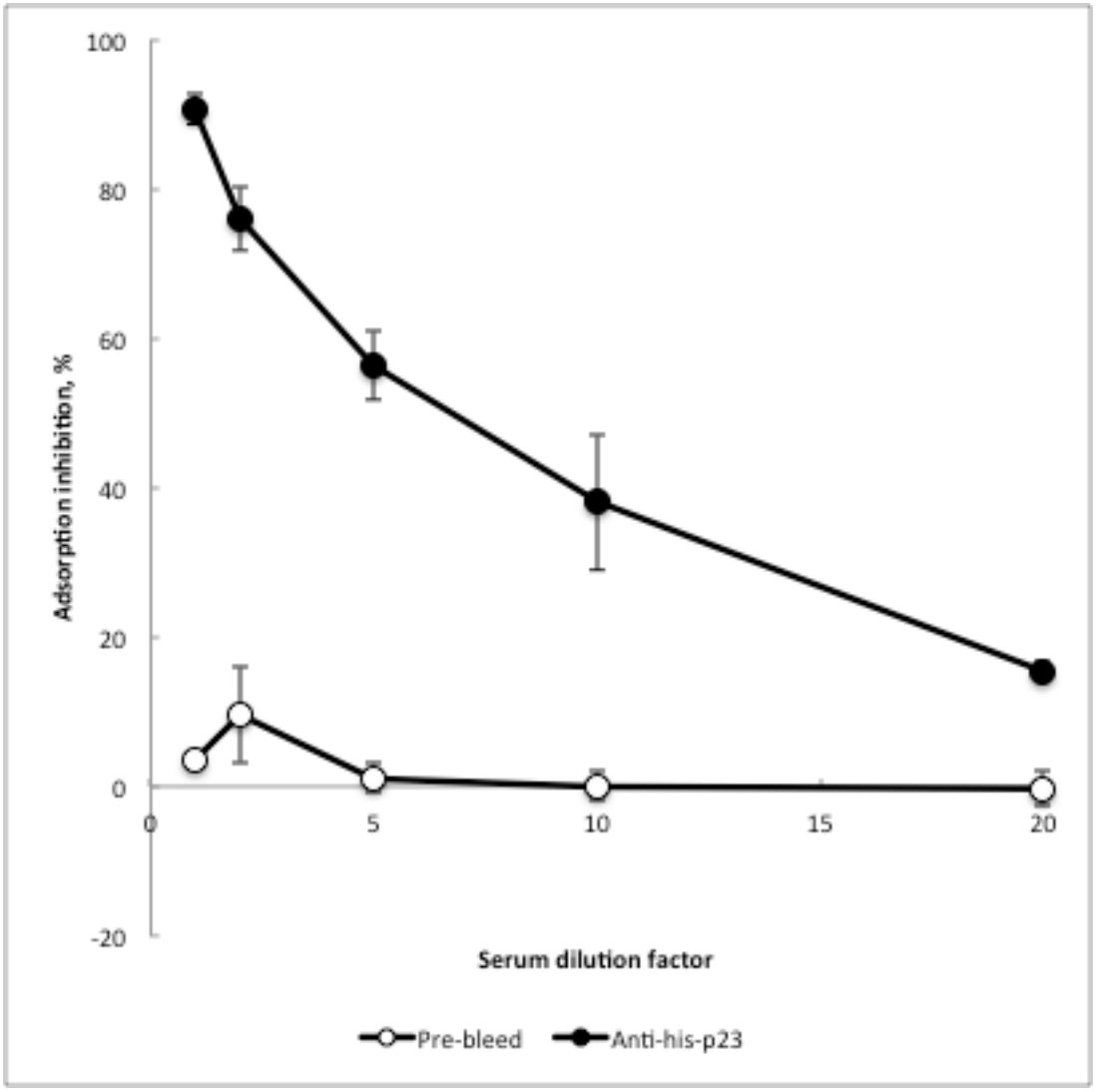

Figure 19. Anti-his-p23 antibody neutralization of Wip1 activity

Polyclonal antibodies were generated against his-p23 and tested for neutralization of Wip1 activity using methods described. After pre-incubation with phage, anti-his-p23 (closed circles) inhibited Wip1 adsorption to *B. anthracis* ΔSterne by up to 90% in a dose-dependent manner. Pre-bleed serum (open circles) did not affect Wip1 adsorption activity. Bars represent standard error of at least 3 experiments.

One explanation for this difference is the possibility that his-p23 is a poor antigen that generated a weak immunogenic response. To test this possibility, an indirect ELISA assay determined that the polyclonal antisera against his-p23 demonstrated reasonable immunogenic strength (reading of Abs=1 at 1:2000 dilution). However, although the antisera was reactive against recombinant his-tagged p23, it still may not exhibit the same level of immunogenicity against non-his-tagged p23 on the Wip1 virion.

Additional observations led us to a second possible explanation. When the serum-phage-bacterium mixtures were pelleted to remove unbound and antibody-bound phage, the adsorption inactivation rate was ~80%. Yet, when the serum-phage-bacterium mixtures were plated directly without pelleting, the same concentration of anti-sera reduced infectivity by only ~40% (Figure 20). From this finding, we hypothesized two possibilities: that Wip1 phage association with the polyclonal antibodies is reversible and/ or that Wip1 phage has a higher affinity for its host receptor than for the polyclonal antibodies generated against his-p23. In an assay with such kinetics, antibody-bound phage plated with bacteria would disassociate from the antibodies over time and preferentially bind to and infect its host instead. In contrast, plating only the pelleted bacterium-bound phage would remove the population of reversibly antibody-bound phage from the assay, allowing for greater sensitivity.

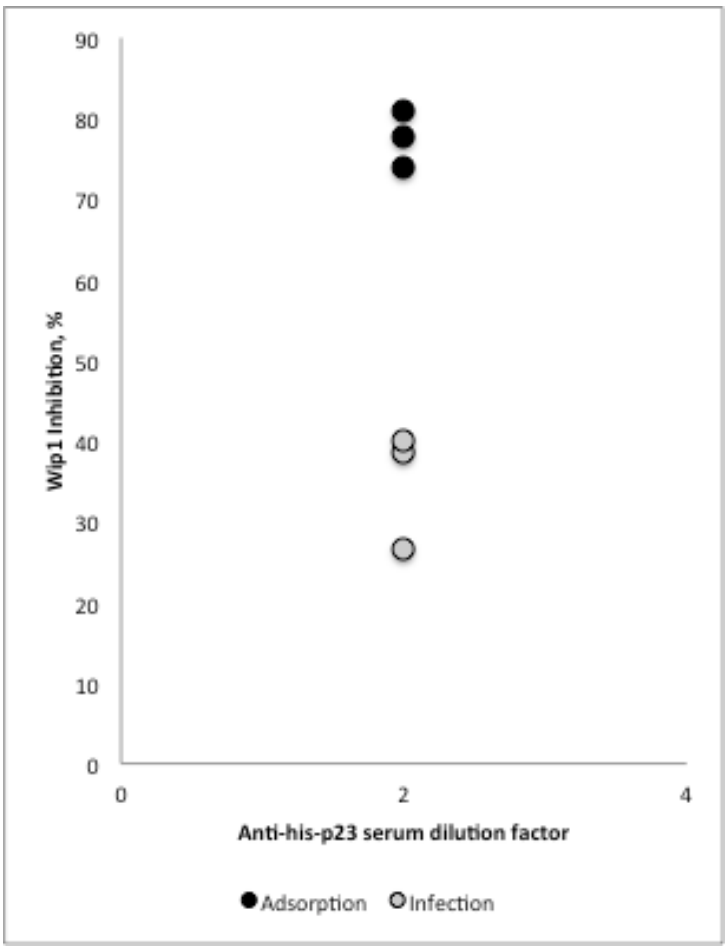

Figure 20. Comparison of anti-his-p23 serum neutralization of Wip1 adsorption and infection

Anti-his-p23 antibodies were tested for inhibition of both Wip1 adsorption (closed circles) and infection (open circles) using the same serum dilution. While anti-his-p23 serum inhibited initial adsorption (~80%), infectivity was inhibited to a much lesser degree (~40%). This suggests that the effects of antibody neutralization become less pronounced over time as phage dissociate from the antibodies and preferentially bind to and infect their hosts.

8. Wip1 p23 binding is specific to *B. anthracis*

To further understand the interaction between Wip1 proteins and bacterial surfaces, the purified his-tagged viral proteins were tested for surface labeling of select bacterial strains using indirect immunofluorescence microscopy. After adherence to a microscope slide, fixed bacterial cells were first labeled with his-tagged recombinant viral proteins, then with anti-his antibodies from mice, and finally with red-fluorescent anti-mouse antibodies (Figure 21). Cells were also stained with 4',6-diamidino-2-phenylindole (DAPI), a blue-fluorescent stain that binds strongly to dsDNA.

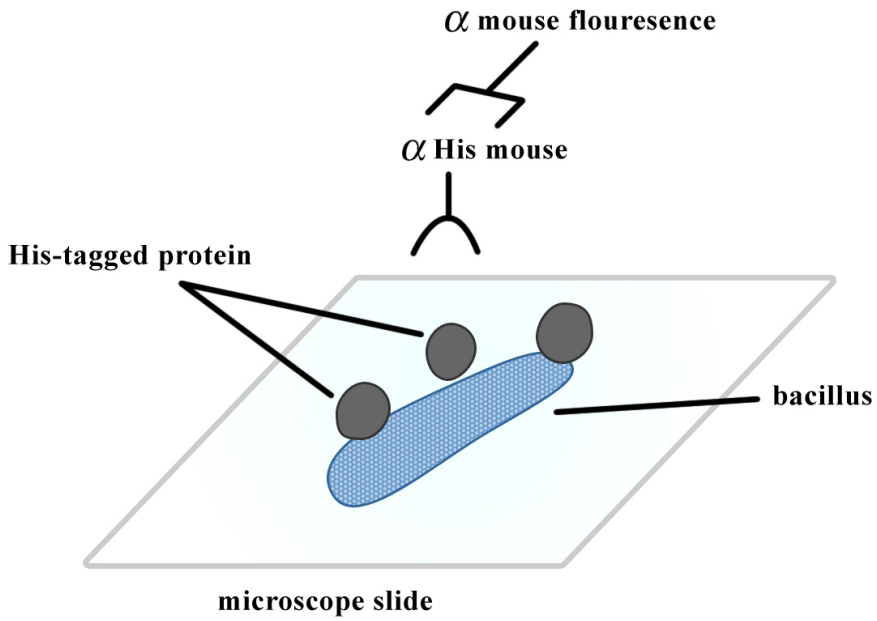

Figure 21. Schematic of multi-step indirect immunofluorescence labeling

Figure 22 illustrates that both his-p23 and the his-p23 + p24 complex bind to the surface of *B. anthracis* ΔSterne. These observations are consistent with Wip1 p23's function as a receptor-binding protein. Surprisingly, the proteins bound all mid-log phase ΔSterne uniformly but bound only a subpopulation of stationary phase ΔSterne. His-p22 and his-p24 were unable to bind either phase of ΔSterne, further suggesting that Wip1 p22 and p24 are not involved with Wip1 adsorption. As expected, no Wip1 proteins bound the surface of *B. cereus* ATCC 4342, which Wip1 neither infects nor adsorbs to.

In Figures 23 and 24, the specificity of the binding of his-p23 and the his-p23 + p24 complex to *B. anthracis* is shown by additional indirect immunofluorescence microscopy. The recombinant viral proteins successfully bound *B. cereus* CDC32805, the only *B. cereus* strain in our host range analysis that supported Wip1 infection and adsorption (Table 4). In contrast, the his-tagged proteins were unable to bind the surface of *B. cereus* strains CDC13100, CDC13140, ATCC 10987, and NRL 569. They were also unable to bind *B. thuringiensis* strains HD1 and HD73. None of these unlabeled strains support either Wip1 infection or adsorption. These findings suggest that his-p23 does not bind to just any gram-positive bacterial surface, but binds very specifically to the bacterial hosts that support Wip1 infection and adsorption, including *B. anthracis* ΔSterne.

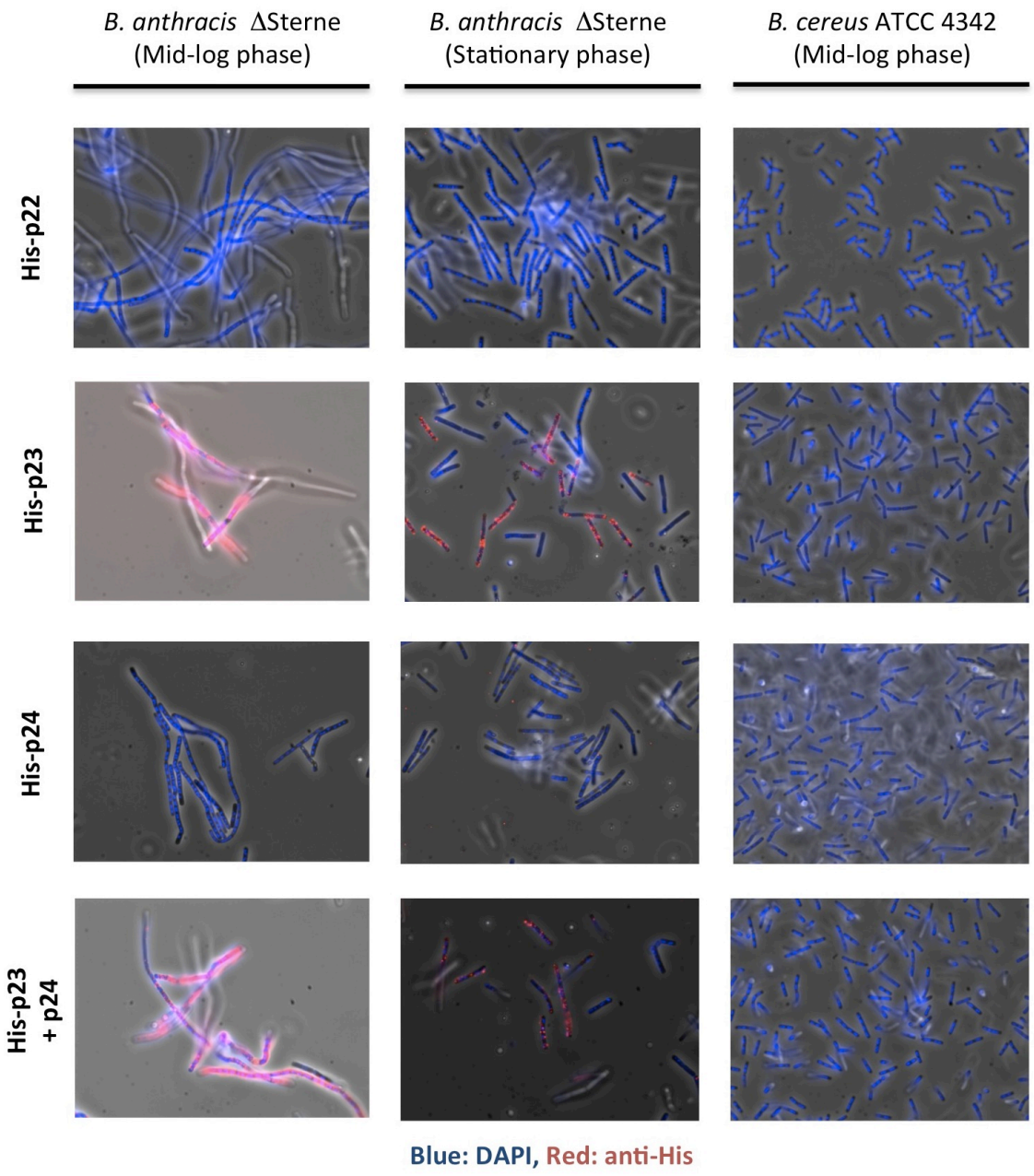

Figure 22. Indirect immunofluorescence microscopy using his-tagged Wip1 proteins

1000X magnification

Table 4. Comparative table of Wip1 host range and his-p23 binding

Bacterial strains that support Wip1 infectivity and adsorption showed positive labeling by immunofluorescent his-p23 and his-p23 + p24 complex. Bacterial strains resistant to Wip1 activity were not labeled by his-p23 or his-p23 + p24 complex. The lower limit of detection of infectivity is indicated by "< 10", while the lower limit of detection of adsorption is indicated by "< 5".

	Infectivity (PFU/ml)		**Adsorption (%)**	**Immunofluorescence**	
Strain/ protein	Wgamma	Wip1	Wip1	his-p23	his-p23 + p24
Bacillus anthracis					
delta Sterne	3.0E+09	6.0E+09	100	+	+
Bacillus cereus					
ATCC 4342	1.0E+05	< 10	< 5	-	-
CDC32805	4.0E+07	3.0E+07	94	+	+
CDC13100	< 10	< 10	< 5	-	-
CDC13140	< 10	< 10	< 5	-	-
ATCC 10987	< 10	< 10	< 5	-	-
NRL 569	< 10	< 10	< 5	-	-
Bacillus thuringiensis					
HD1	< 10	< 10	< 5	-	-
HD73	< 10	< 10	< 5	-	-

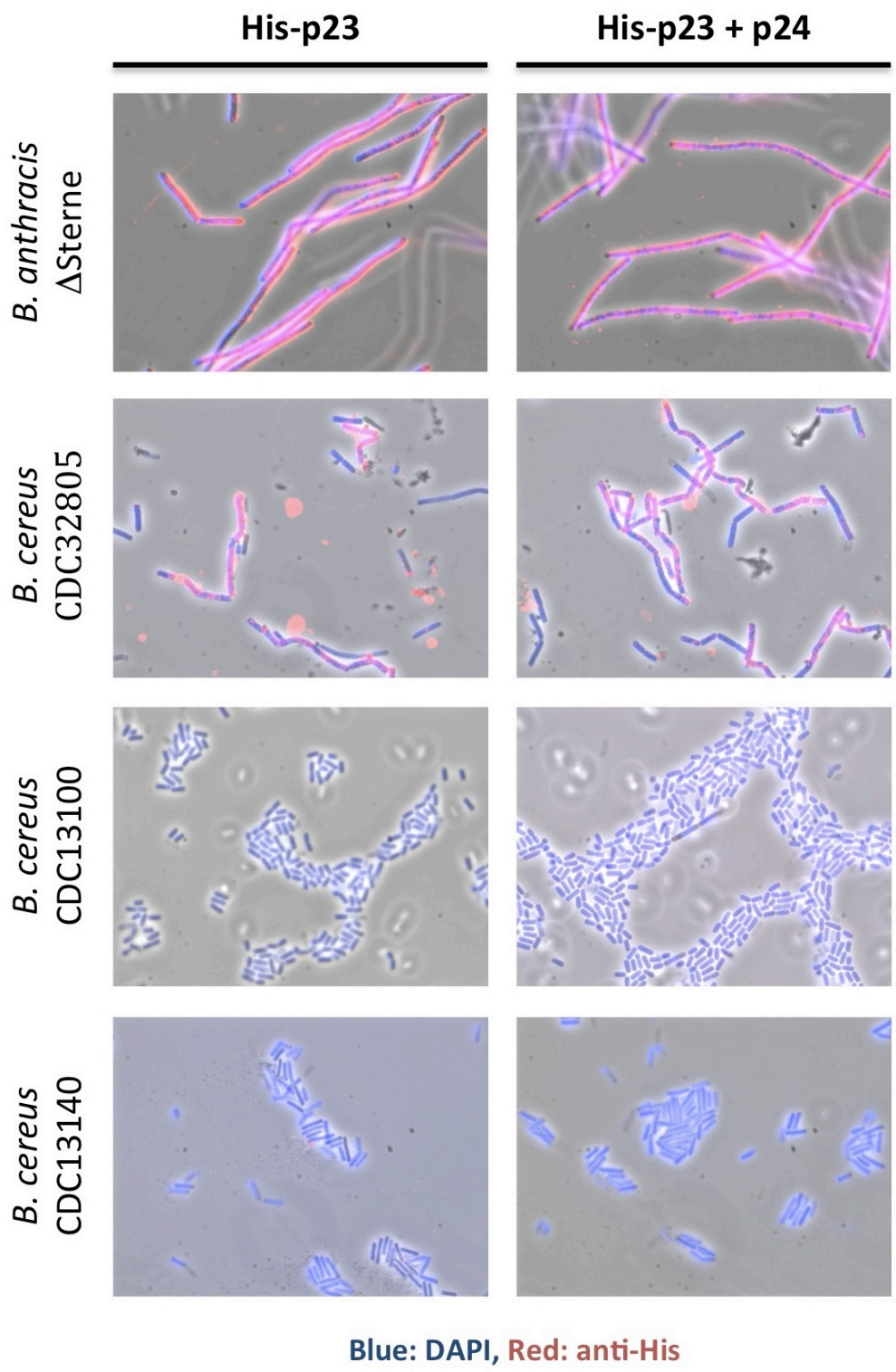

Figure 23. Indirect immunofluorescence microscopy using his-p23 and the his-p23 + p24 complex 1000X magnification

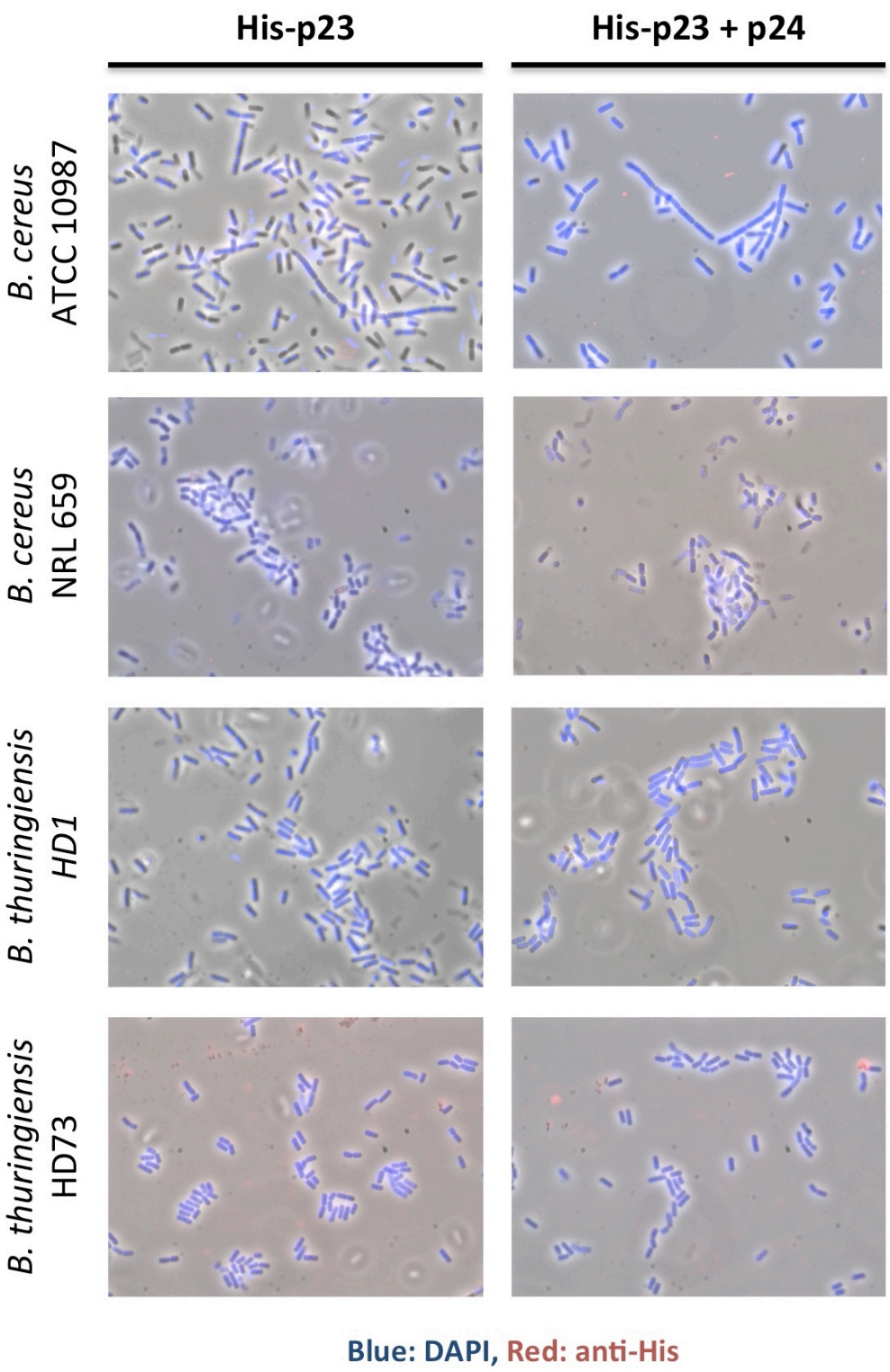

Figure 24. Indirect immunofluorescence microscopy using his-p23 and the his-p23 + p24 complex (cont'd) 1000X magnification

9. *B. anthracis* receptor for Wip1 requires Sap for cell wall presence

Based on Wip1 phage's high specificity for *B. anthracis*, we hypothesized that the cellular receptor for Wip1 is a cell wall component unique to the surface of *B. anthracis*. Teichoic acids and S-layer carbohydrates were not considered to be receptor candidates because they are not present on the surface of *B. anthracis* [68]. The major repeating peptidoglycan components were also eliminated as candidates because they are universally present on all gram-positive bacteria and would not confer host range specificity. In order to identify the cellular Wip1 receptor, we focused our attention on cell wall associated proteins and carbohydrates.

Cell wall associated carbohydrates from *B. anthracis* ΔSterne and *B. cereus* ATCC 4342 were extracted and purified using a hydrofluoric acid treatment as described in the Methods section. These surface carbohydrate fractions were resuspended at a concentration of 8 mg/ml. To study the effect of the carbohydrates on Wip1 activity, the carbohydrate samples were pre-incubated with various dilutions of phage before the mixtures were titered on *B. anthracis* ΔSterne (Figure 25). In this assay, carbohydrate to phage ratios ranged from 0.8 mg carbohydrate sample per 100 PFU Wip1 to 0.8 mg carbohydrate sample per 100,000 PFU Wip1. Phage infectivity was calculated as the percentage of infectious phage out of total phage (as determined by a buffer only control).

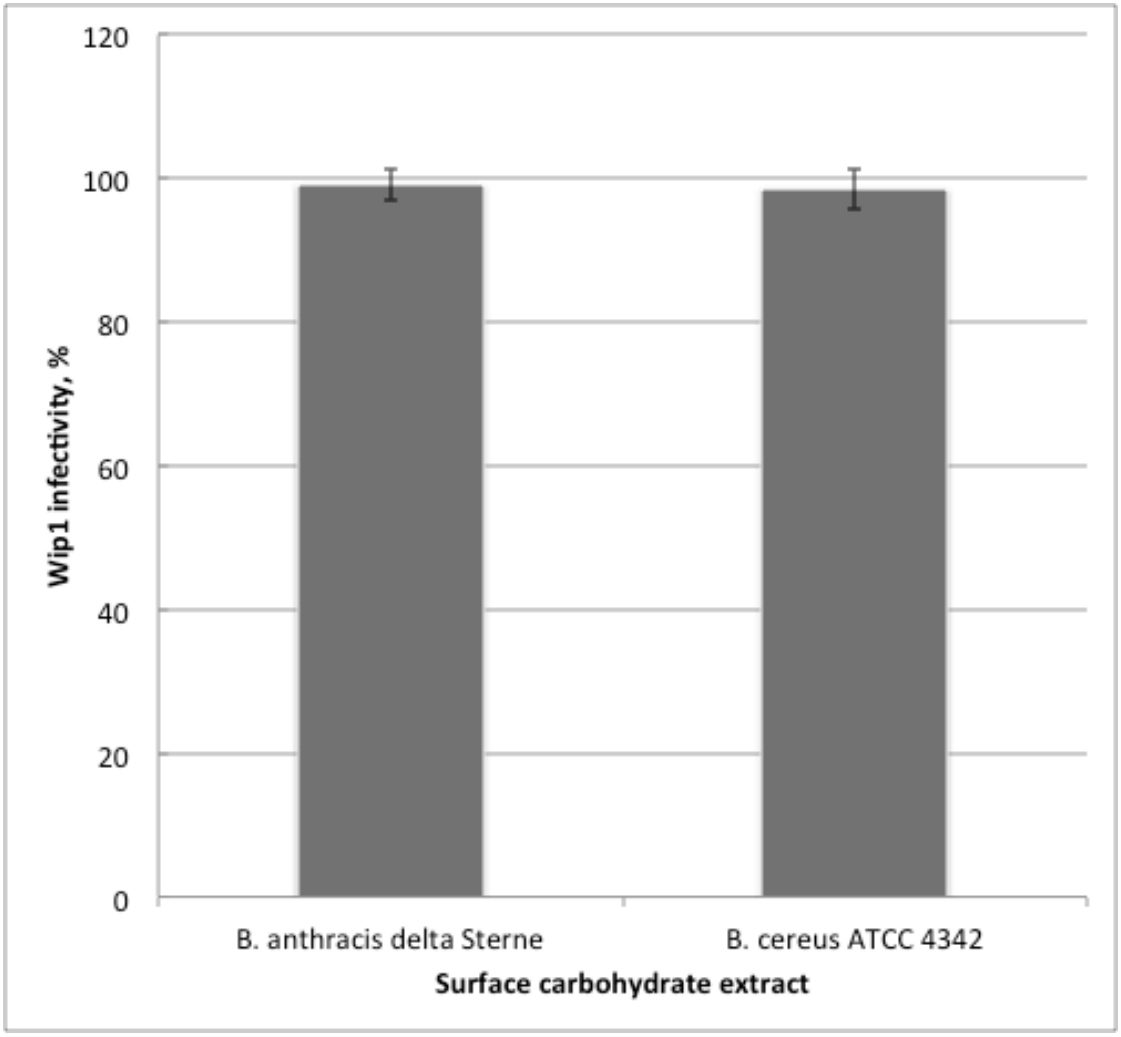

Figure 25. Effect of surface carbohydrates on Wip1 infectivity

Extracted cell wall associated carbohydrates from *B. anthracis* ΔSterne and *B. cereus* ATCC 4342 were tested for their effect on Wip1 infectivity. Various dilutions of phage were pre-incubated with carbohydrate samples before being plated out on ΔSterne. Neither carbohydrate fraction had an effect on Wip1 infectivity in this assay. Bars represent standard errors of 4 separate experiments.

Neither carbohydrate sample from the *Bacillus* strains demonstrated an effect on Wip1 infectivity (Figure 25). However, these results do not necessarily indicate that cell wall associated carbohydrates are not the Wip1 receptor. It should be noted that the carbohydrate extracts were not tested for composition and could possibly lack purity that affected assay results. Furthermore, it is very possible that the assay was not sensitive enough to detect any inhibitory effect of the carbohydrate samples. In order for the assay to detect competitive inhibition, there must be a high enough concentration of receptors to occupy all 11 labile spikes on each Wip1 virion. The results of the carbohydrate inhibition assay were thus deemed inconclusive.

In order to determine if the Wip1 receptor is a bacterial surface protein, we studied the effect of bacterial protease treatment on phage adsorption. Proteases (Pronase and protease K) were incubated with bacterial cells for 1 hour and then removed with multiple washes. Treated and untreated *B. anthracis* ΔSterne and *B. cereus* ATCC 4342 cells were incubated with Wip1 phage for 5 or 20 minutes before centrifugation and spin filtration. Unbound phages present in the supernatant were titered on ΔSterne. Bound phage was calculated as the percentage of adsorbed phage (# total phage - # titered unbound phage in supernatant) out of total phage (as determined by a buffer only control). Adsorption rates measured over 99% for both protease treated and untreated *B. anthracis* cells. The observation that protease treatment of the bacterial surface had no effect on adsorption suggests that the Wip1 receptor is not a surface protein.

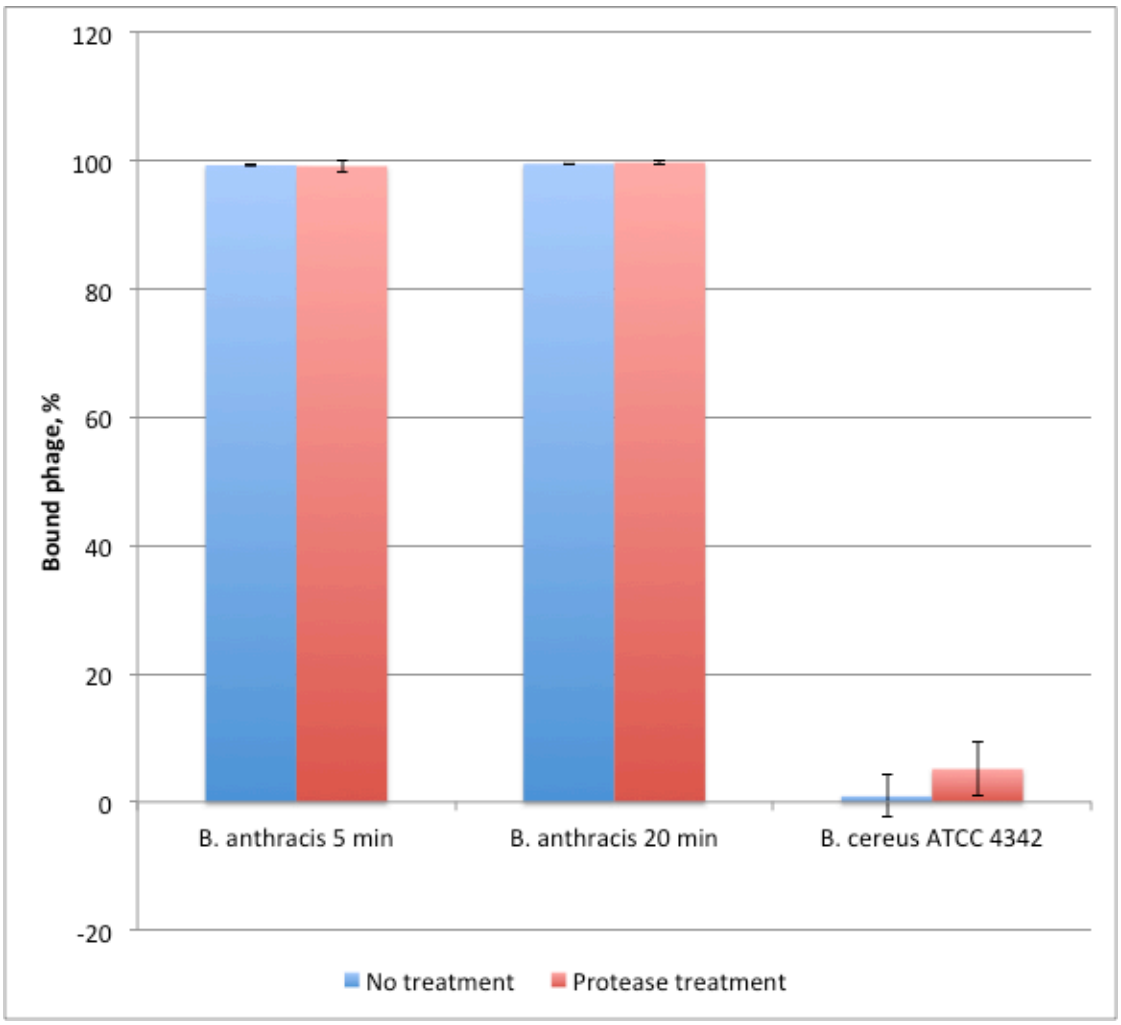

Figure 26. Adsorption to protease treated bacteria

B. anthracis ΔSterne and *B. cereus* ATCC 4342 were treated with and without protease before subsequent washings and incubation with Wip1 phage. Adsorption was measured at 5 and 20 minutes post infection time points. Results indicated no effect on adsorption from protease treatment of cells. Bars represent standard error calculated from at least three separate experiments.

From personal communications, we learned that the closely related phage AP50 does not infect *B. anthracis* SAP- mutants. *SAP* is the gene encoding Sap protein, the 94 kDa *B. anthracis* surface array protein that forms the S-layer during exponential growth [69]. The gene *csaB* lies next to the SAP operon and is required for Sap protein retention on the cell wall. Wip1 was tested for infectivity and adsorption on both *B. anthracis* Sterne SAP- and *B. anthracis* csaB- strains. Infectivity was measured by directly titering Wip1 phage on bacterial soft agar plates. Adsorption was calculated as the percentage of bound phage (# total phage - # unbound phage in supernatant) out of total phage. Both mutants were resistant to Wip1 infection and adsorption (Table 5). This finding indicates that the *B. anthracis* receptor for Wip1 requires Sap protein for its presence on the cell wall.

Indirect immunofluorescence microscopy using his-tagged viral proteins showed that his-p23 and the his-p23 + p24 complex were unable to bind *B. anthracis* Sterne SAP- mutants (Figure 27). This is consistent with the hypothesis that this mutant lacks the Wip1 receptor on its surface.

Table 5. *B. anthracis* Sap mutants do not support Wip1 infection or adsorption

	Infectivity (PFU/ml)	Adsorption (%)	Immunofluorescence		
Strain/ protein	Wip1	Wip1	his-p23	his-p24	his-p23 + p24
Bacillus anthracis					
Sterne	1.5E+10	100	+	-	+
Sterne SAP-	< 10	< 5	-	-	-
Sterne csaB-	< 10	< 5			

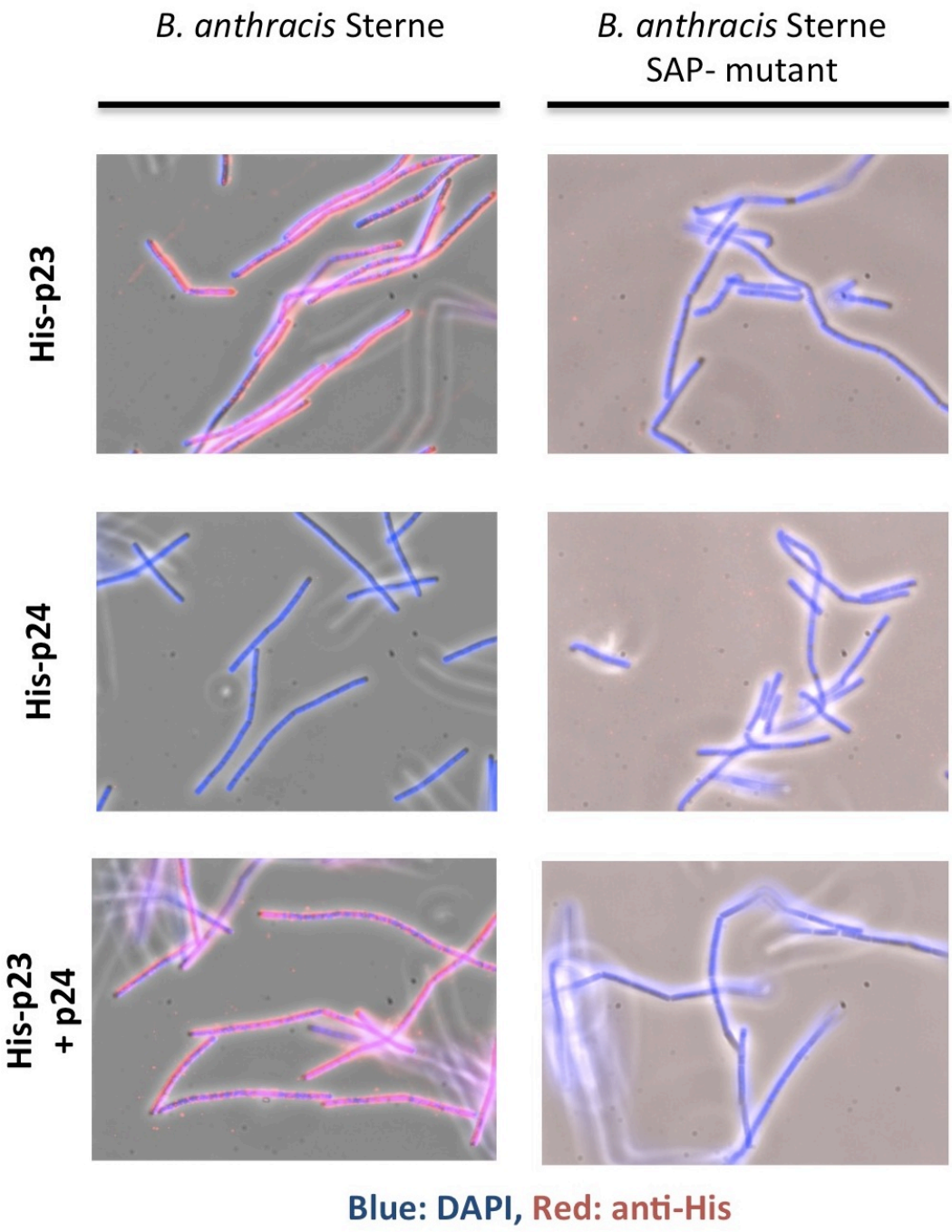

Figure 27. Indirect immunofluorescence microscopy on *B. anthracis* Sterne SAP- mutants using his-tagged Wip1 proteins

1000X magnification

In order to test whether the Sap protein itself was the Wip1 receptor, we performed a pull-down assay using receptor-binding complex his-p23 + p24 as the affinity ligand. Cell wall associated proteins were extracted from mid-log phase *B. anthracis* ΔSterne and *B. cereus* ATCC 4342 by incubating the cells with PlyG lysin in a 30% raffinose solution. While PlyG normally lyses *Bacillus* cells, the 30% raffinose solution keeps the protoplasm intact, preventing the release of cytoplasmic proteins into solution. After the protoplasms were pelleted, the cell wall associated proteins in the supernatant were applied to a Ni-NTA column pre-loaded with the receptor-binding complex his-p23 + p24. Fractions from the column flow-throughs, washes, and elution were collected, concentrated using TCA precipitation, and analyzed with SDS-PAGE.

Sap protein was revealed in fractions from mid-log phase *B. anthracis* ΔSterne but not *B. cereus* ATCC 4342. However, the Sap protein was not present in the elution, indicating that Sap did not bind to the receptor-binding complex in the pull-down assay (Figure 28). Surprisingly, the elutions from both ΔSterne and ATCC 4342 pull-down assays contained two non-viral proteins measuring between 30 to 40 kDa. However, these proteins were not pulled down during the assay as they were revealed to be present in TCA concentrated samples of purified his-p23 + p24 complex stock. Since the recombinant proteins were expressed using *E. coli* cells, these two proteins were not considered candidates for the *B. anthracis* specific cellular receptor for Wip1.

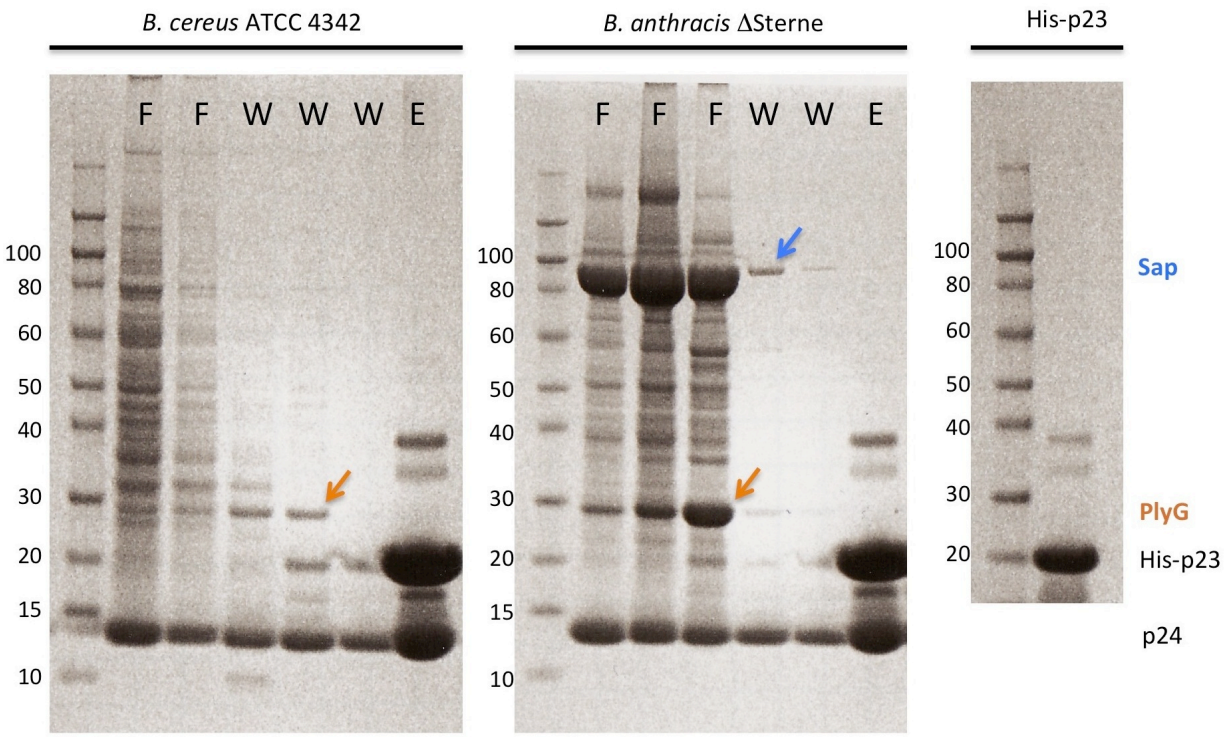

Figure 28. Pull-down assay using receptor-binding complex his-p23 + p24

Cell wall associated proteins from mid-log phase *B. anthracis* ΔSterne and *B. cereus* ATCC 4342 were applied to Ni-NTA columns pre-loaded with the receptor-binding complex his-p23 + p24. Fractions of the flow-throughs (F), washes (W), and elution (E) were collected and analyzed with SDS-PAGE. 26 kDa PlyG (orange arrows) was used in the surface protein extraction method. 94 kDa Sap protein (blue arrow) was identified in ΔSterne flow-through and wash fractions, but was not eluted with the receptor-binding complex. The elution fraction revealed two proteins between 30 - 40 kDa that were also present in the his-p23 + p24 protein stock sample.

The results of the pull-down assay strongly suggest that Sap protein is not a receptor for Wip1 phage. The lack of proteins pulled down in the assay was also consistent with the previous finding that the receptor is not a protein. Although the cellular receptor for Wip1 has yet to be identified, it has been thus characterized as a cell wall component specific to the *B. anthracis* surface that requires Sap protein for surface availability.

D. DISCUSSION

Isolated relatively recently in 2003, Wip1 phage is the newest member of the rare *Tectiviridae* family. Tectiviruses have been of particular interest due to PRD1's structural similarities to the mammalian adenovirus and AP50's high specificity for the biowarfare pathogen *B. anthracis*. Interestingly, Wip1 also exhibits a narrow host range that is highly specific for *B. anthracis*, more so than the current diagnostic standard Wγ phage [1]. In the present study, we determined with adsorption assays that specificity to *B. anthracis* is mediated by Wip1's receptor-binding ligand. Here, we reported the unusual Wip1 genomic sequence and identified Wip1 gene product 23 as a receptor-binding protein. We also showed that Wip1 p23 forms a complex with another viral protein p24 and binds very specifically to *B. anthracis*. Ultimately, we demonstrated that Wip1 is a unique phage and characterized the molecules determining its host tropism.

1. Wip1 specificity for *B. anthracis* is mediated by specificity of adsorption

Wip1 exhibits a highly specific tropism for *B. anthracis* and does not infect closely related *Bacillus* strains such as *B. cereus* ATCC 4342. Although tropism is often determined by receptor binding, this is not always the case. For example, the poliovirus receptor is not sufficient to determine poliovirus tropism to the brain and spinal cord since this protein receptor is produced on a broad range of animal tissues. Instead, restriction of poliovirus replication is thought to occur after viral binding and entry [76, 77]. In another case, electron microscopy showed that Wγ phage binds to the surface of *B. thuringiensis* 97-27, a strain that it does not infect [61]. This finding indicates that the Wγ receptor GamR is sufficient for binding but not for DNA delivery.

By testing closely related *Bacillus* strains for Wip1 adsorption, we demonstrated that Wip1 binding is very specific to *B. anthracis* (Table 2). This strongly suggests that Wip1 specificity for *B. anthracis* infection is indeed mediated by specificity of adsorption. Additionally, adsorption kinetics indicated that Wip1 binding to its host surface is both specific and rapid. *B. anthracis* ΔSterne bound 80% of virus particles within one minute (Figure 9). This rapid adsorption is also observed during Bam35 binding to *B. thuringiensis* HER1410 [39]. However, given that the Bam35 receptor is a major peptidoglycan component that dominates the cell surface, these kinetics are less surprising for Bam35 than for Wip1.

2. Wip1 sequence exhibits both tectiviral genome conservation and notable distinctions

We sequenced and examined the Wip1 sequence and determined that it shares significant similarities to the genomes of other gram-positive infecting tectiviruses. Its genome length of 14,319 bp is close to other tectiviral genome lengths ranging from 14,398 bp (AP50) to 14,925 bp (PRD1). The map of Wip1's 27 putative ORFs reveal a tightly packed organization with short genes and few noncoding regions, characteristic of all tectiviral genomes (Figure 12). The Wip1 genome is predicted to encode a Lex-A-type regulator, five DNA packaging/ assembly genes, a DNA delivery gene, two lysins, and at least four capsid/ spike genes. The size, sequence, and/ or organization of these ORFs are remarkably similar to that of other gram-positive infecting tectiviruses. Wip1 is most closely related to *B. anthracis* specific phage AP50, with 15 out of 27 ORFs sharing sequence identity of at least 75% to corresponding AP50 genes.

While the central section of the Wip1 genome exhibits some conservation to other tectiviral genomes, the extremities displayed highly unusual features. This was rather unexpected considering that all other gram-positive infecting tectiviruses exhibited significant conversation throughout the entire lengths of their genomes. In fact, Bam35, GIL01, and GIL16 share 86 to 99% sequence similarity. In contrast, Wip1 is missing the first 5 conserved ORFs and has replaced them with unique genes for ORFs 1 through 4. Most interestingly, Wip1 encodes its DNA polymerase at the very end of its genome

on the negative strand whereas all other tectiviruses including PRD1 encode its polymerase early in the sequence on the positive strand. Furthermore, many of these genes are not only unique within the group but also unique within the entire known database of proteins.

Notably, the GC content at both extremities is lower than the percentage observed in the central region of the genome and more precisely, in all the ORFs that share homology with AP50 (Table 3). The 5' end of the Wip1 genome encodes ORFs 1 through 4, which have GC contents of 29.5%, 30.7%, 25.7%, and 25.7%, respectively. The opposite 3' end encodes ORF27 which has a GC content of 29.7%. In contrast, the genes located at the center, such as ORF18 and ORF19, have GC contents of 43.1% and 44.8%, respectively. Intergenic spaces at the extremities are also larger than those at the central section of its own sequence and what is observed for other tectiviral genomes. These observations point to the possibility of a different origin for the genome extremities of Wip1. The combination of conservation and deviation exhibited could indicate that Wip1 is an evolutionary hybrid between AP50 and something else with significant differences.

3. Wip1 receptor-binding ligand p23 is a unique protein

The identification of Wip1 p23 as a receptor binding protein is very interesting because it is a unique protein with no homology to any other known proteins. It is particularly surprising because ORF23 shares no sequence identity with AP50, a closely related tectivirus with a similar host range that is also highly specific to *B. anthracis*. Genomic analysis showed that the overall Wip1 genome shares significant similarities to the AP50 genome in ORF size, sequence, and organization. In fact, the genes neighboring Wip1 ORF23 display this conservation. ORF22 (291 residues) shares 84% sequence identity with AP50 ORF27 (304 residues) and ORF24 (118 residues) shares 51% sequence identity with AP50 ORF29 (118 residues).

Another interesting observation is that AP50 ORF28, which is located in the corresponding genomic position to Wip1 ORF23, is the gene that harbors one of two sequence mutations that differentiate isolates AP50t, which produces turbid plaques, and AP50c, which produces clear plaques [41]. Generally, clear plaques are formed when the host is completely susceptible to the phage while turbid plaques are formed if the host is partially resistant to the phage (e.g. if 10% of the cells survive infection). The other mutation is located in the non-coding region upstream of ORF1. Furthermore, AP50 ORF28 and Wip1 ORF23 are located at a highly variable region of their respective genomes. On the one hand, it is not too surprising that the Wip1 receptor-binding domain ORF23 exhibits sequence diversity. On the other

hand, it is rather unusual that two closely related tectiviruses with a similar host range have evolved uniquely different receptor binding proteins.

4. A proposed function for Wip1 p24

A notable observation is that the his-p23 + p24 complex exhibited higher competitive inhibition than his-p23 alone (Figure 18), suggesting that p24 somehow complemented or enhanced his-p23 binding activity. This enhancement could result from simply protecting his-p23 proteins from degradation. However, we were careful to use fresh protein stocks in the assay. Considering that the inhibition rate of his-p23 was dose-dependent, the increased inhibitory activity from the complex sample could simply result from higher amounts of the his-p23 protein. However, SDS-PAGE analysis of the recombinant protein stocks used in the assay (Figure 15) showed that this was not the case.

Another more interesting possibility is that p24 plays a secondary but complementary role in Wip1 binding. The adsorption of phage to the gram-positive bacterial surface has been suggested to occur in two stages. The first step involves reversible binding to general recognition molecules on the cell surface. This weak interaction allows the virion to stay close to the bacterial surface while diffusing across space. The second step involves colliding with a specific receptor in an irreversible manner. The seahorse-like structure for PRD1 receptor-binding protein P2 consists of multiple domains with different

purported functions [4]. In one P2 model, the fin-shaped domain is proposed to make initial contacts by scanning the host surface in order to bring the receptor-binding domain closer to its receptor. It is possible that Wip1 p24 is such a spike complex domain with non-specific, reversible surface scanning properties.

5. Considerations regarding the Sap-dependent cellular receptor

The inability of Wip1 phage to adsorb to or infect *B. anthracis* Sterne SAP- and csaB- mutants indicated that the cellular receptor requires Sap protein on the cell surface. The *SAP* gene encodes the Sap protein and the neighboring *csaB* gene is involved in anchoring Sap protein to the cell wall. The observation that Wip1 binding is Sap dependent led to many questions.

First, we wondered about Wip1 adsorption to and his-p23 binding to stationary phase *B. anthracis* ΔSterne cells. In *B. anthracis*, Sap decorates the bacterial surface only during exponential growth and is subsequently replaced by S-layer protein EA1 upon entering stationary phase [71]. Adsorption assays were conducted using stationary *B. anthracis* ΔSterne cells and, yet, we observed rapid adsorption of 80% of virions after one minute and up to 99% after 10 minutes (Figure 9). Similarly, indirect immunofluorescence microscopy showed his-p23 binding to fixed stationary phase ΔSterne (Figure 22). Interestingly, the viral ligand was only able to bind to a subpopulation of stationary phase ΔSterne but was able to bind all mid-log phase ΔSterne.

Additionally, the signal from his-p23 labeling was noticeably stronger for mid-log phase ΔSterne than for stationary phase cells.

The ability of stationary phase *B. anthracis* lacking Sap protein to adsorb the Wip1 receptor-binding ligand could possibly be explained by the highly flexible regulatory mechanism of *SAP* and *ea1* expression. Although Sap is replaced by EA1 during stationary phase, it was also observed that Sap is readily expressed as soon as stationary phase cells were resuspended in fresh medium [71]. It should be noted that while the indirect immunofluorescence microscopy methods involved cell washing before fixation, the adsorption assay did not involve any wash steps, only the addition of propagated phage stored in a mixture of BHI media and buffer. As flexible as sap regulation may be, it remains curious that unwashed stationary *B. anthracis* cells were observed to adsorb 80% of virions in one minute.

A second question we wondered was whether Sap protein itself was the actual receptor. Although the protease treatment assay seemed to suggest that the receptor was not proteinaceous in nature, the new considerations regarding the rapid production of Sap made this assay inconclusive. However, Sap protein extracted from the surface of mid-log phase *B. anthracis* ΔSterne did not exhibit affinity to the receptor-binding complex in the pull down assay. While the protease assay was deemed inconclusive in light of new observations, the pull down assay results still indicated that Sap was not a receptor for the Wip1 his-p23 + p24 complex.

A third question we asked was regarding the nature of the Sap dependent receptor. Curiously, the S-layer for *B. anthracis* is not decorated with carbohydrate residues and Sap layer-associated proteins have not been described. While the receptor has yet to be identified, it would be very interesting indeed to characterize a *B. anthracis*-specific cell wall element that requires Sap protein for availability on the cell surface.

6. Wip1 phage potential as a diagnostic tool for *B. anthracis*

The Wip1 phage and its receptor-binding ligand exhibit promise as bio-defense tools in the detection of the Category A pathogen *B. anthracis*. We demonstrated that not only does Wip1 infect *B. anthracis* with high specificity, but it also binds to its surface in a manner that is remarkably rapid and exhibits high affinity. Indirect immunofluorescence microscopy demonstrated that the Wip1 receptor-binding p23 and the p23+p24 complex detect and bind *B. anthracis* with specificity that seems to match its narrow host range. In addition to high specificity, we propose that the receptor-binding p23 exhibits higher affinity for its receptor than to even polyclonal antibodies generated against it. These characteristics that we report here make Wip1 and its receptor-binding ligand potentially useful diagnostic tools for *B. anthracis*.

E. REFERENCES

1. Schuch, R., et al., *Prevalence of Bacillus anthracis-like organisms and bacteriophages in the intestinal tract of the earthworm Eisenia fetida.* Applied and environmental microbiology, 2010. **76**(7): p. 2286-94.

2. Huiskonen, J.T., V. Manole, and S.J. Butcher, *Tale of two spikes in bacteriophage PRD1.* Proceedings of the National Academy of Sciences of the United States of America, 2007. **104**(16): p. 6666-71.

3. Rydman, P.S., et al., *Bacteriophage PRD1 contains a labile receptor-binding structure at each vertex.* J. Mol. Biol., 1999. **291**: p. 575-587.

4. Xu, L., et al., *The Receptor Binding Protein P2 of PRD1, a Virus Targeting Antibiotic-Resistant Bacteria, Has a Novel Fold Suggesting Multiple Functions.* Structure, 2003. **11**: p. 309-322.

5. Ackermann, H.W., *Frequency of morphological phage descriptions in the year 2000.* Arch Virol, 2001. **146**(5): p. 843-857.

6. Travis, J., *All the World's a Phage.* Science News, 2003. **164**(2): p. 26-28.

7. Espejo, R.T. and E.S. Canelo, *Origin of Phospholipid in Bacteriophage PM2.* Journal of virology, 1968. **2**(11): p. 1235-1240.

8. Borriss, M., et al., *Isolation and characterization of marine psychrophilic phage-host systems from Artic sea ice.* Extremophiles, 2003. **7**(5): p. 377-384.

9. Olsen, R.H., J. Siak, and R.H. Gray, *Characteristics of PRD1, a Plasmid-Dependent Broad Host Range DNA Bacteriophage.* Journal of Virology, 1974. **14**(3): p. 689-699.

10. Prigent, M., et al., *A diversity of bacteriophage forms and genomes can be isolated from the surface sands of the Sahara Desert.* Extremophiles, 2005. **9**(4): p. 289-296.

11. Breitbart, M.B., et al., *Phage Community Dynamics in Hot Springs.* Applied and environmental microbiology, 2004. **70**(3): p. 1633-1640.

12. Marks, T. and R. Sharp, *Bacteriophages and biotechnology: a review.* Journal of chemical technology and biotechnology, 2000. **75**(1): p. 6-17.

13. Summers, W.C., *Bacteriophage Therapy.* Annual review of microbiology, 2001. **55**: p. 437-451.

14. Cairns, J., G.S. Stent, and J.D. Watson, eds. *Phage and the Origins of Molecular Biology*. 1992, Cold Spring Harbor Laboratory Press.

15. O'Neil, K.T. and R.H. Hoess, *Phage display: protein engineering by directed evolution.* Curr Opin Struct Biol, 1995. **5**(4): p. 443-449.

16. Abshire, T.G., J.E. Brown, and J.W. Ezzell, *Production and validation of the use of gamma phage for identification of Bacillus anthracis.* Journal of clinical microbiology, 2005. **43**(9): p. 4780-8.

17. Bradley, D.E. and E.L. Rutherford, *Basic characterization of a lipid-containing bacteriophage specific for plasmids of the P, N, and W compatibility groups.* Canadian Journal of Microbiology, 1975. **21**(2): p. 152-163.

18. Stanisich, V.A., *The properties and host range of male-specific bacteriophages of Pseudomonas aeruginosa.* J. gen. microbiol, 1974. **84**(2): p. 332-342.

19. Wong, F.H. and L.E. Bryan, *Characteristics of PR5, a lipid-containing plasmid-dependent phage.* Canadian Journal of Microbiology, 1978. **24**(7): p. 875-882.

20. Coetzee, W.F. and P.J. Bekker, *Pilus-specific, lipid-containing bacteriophages PR4 and PR772: comparison of physical characteristics of genomes.* J. gen. Virol., 1979. **45**(1): p. 195-200.

21. Saren, A., et al., *A Snapshot of Viral Evolution from Genome Analysis of the Tectiviridae Family.* Journal of Molecular Biology, 2005. **350**: p. 427-440.

22. Ackermann, H.W., et al., *Partial Characterization of a Cubic Bacillus Phage.* Canadian Journal of Microbiology, 1978. **24**: p. 986-993.

23. Nagy, E.P., B.; Ivanovics, G., *Characteristics of Phage AP50, an RNA Phage Containing Phospholipids.* Journal of General Virology, 1976. **32**: p. 129-132.

24. Sakaki, Y., et al., *Bacteriophage phiNS11: a lipid-containing phage of acidophilic thermophilic bacteria.* J. Biochem, 1977. **82**(5): p. 1451-1456.

25. Verheust, C., G. Jensen, and J. Mahillon, *pGIL01, a linear tectiviral plasmid prophage originating from Bacillus thuringiensis serovar israelensis.* Microbiology, 2003. **149**(8): p. 2083-2092.

26. Verheust, C., N. Fornelos, and J. Mahillon, *GIL16, a new gram-positive tectiviral phage related to the Bacillus thuringiensis GIL01 and the Bacillus cereus pBClin15 elements.* Journal of bacteriology, 2005. **187**(6): p. 1966-1973.

27. Rydman, P.S. and D.H. Bamford, *The Lytic Enzyme of Bacteriophage PRD1 Is Associated with the Viral Membrane.* Journal of bacteriology, 2001. **184**(1): p. 104-110.

28. Bamford, D.H., J. Caldenty, and J.K. Bamford, *Bacteriophage PRD1: a broad host range dsDNA tectivirus with an internal membrane.* Adv Virus Res, 1995. **45**: p. 281-319.

29. Bamford, D.H., et al., *Comparison of the Lipid-containing Bacteriophages PRD1, PR3, PR4, PR5, and L17.* J. gen. Virol., 1981. **57**: p. 365-373.

30. Bamford, D., *Evolution of Viral Structure.* Theoretical Population Biology, 2002. **61**(4): p. 461-470.

31. Merckel, M.C., et al., *The Structure of the Bacteriophage PRD1 Spike Sheds Light on the Evolution of Viral Capsid Architecture.* Molecular Cell, 2005. **18**: p. 161-170.

32. Grahn, A.M., et al., *Stable Packaging of Phage PRD1 DNA Requires Adsorption Protein P2, Which Binds to the IncP Plasmid-Encoded Conjugative Transfer Complex.* Journal of bacteriology, 1999. **181**(21): p. 6689-6696.

33. Mindich, L.B., D.; McGraw, T.; Mackenzie, G, *Assembly of bacteriophage PRD1: particle formation with wild-type and mutant viruses.* Journal of virology, 1982. **44**(3): p. 1021-1030.

34. Grahn, A.M., R. Daugelavicius, and D.H. Bamford, *Sequential model of phage PRD1 DNA delivery: active involvement of the viral membrane.* Mol. Microbiol., 2002. **46**: p. 1199-1209.

35. Lundstrom, K.H., et al., *Lipid-containing bacteriophage PR4: structure and life cycle.* J. gen. Virol., 1979. **43**(3): p. 583-592.

36. Laurinmaki, P.A., et al., *Membrane Proteins Modulate the Bilayer Curvature in the Bacterial Virus Bam35.* Structure, 2005. **13**: p. 1819-1828.

37. Ravantti, J.J., et al., *Comparative analysis of bacterial viruses Bam35, infecting a gram-positive host, and PRD1, infecting gram-negative hosts, demonstrates a viral lineage.* Virology, 2003. **313**: p. 401-414.

38. Stromsten, N.J., et al., *The Bacillus thuringiensis Linear Double-Stranded DNA Phage Bam35, Which Is Highly Similar to the Bacillus cereus Linear Plasmid pBClin15, Has a Prophage State.* Journal of bacteriology, 2003. **185**(23): p. 6985-6989.

39. Gaidelyte, A., et al., *The Entry Mechanism of Membrane-Containing Phage Bam35 Infecting Bacillus thuringiensis.* Journal of bacteriology, 2006. **188**(16): p. 5925-5934.

40. Nagy, E. and G. Ivanovics, *Anthrax-specific "AP-50-like" phages isolated from Bacillus cereus strains.* Acta Microbiol Acad Sci Hung, 1982. **29**(2): p. 89-98.

41. Sozhamannan, S., et al., *Molecular Characterization of a Variant of Bacillus anthracis-Specific Phage AP50 with Improved Bacteriolytic Activity.* Applied and environmental microbiology, 2008. **74**(21): p. 6792-6796.

42. Nagy, E. and G. Ivanovics, *Association of probable defective phage particles with lysis by bacteriophage AP50 in Bacillus anthracis.* J. gen. microbiol, 1977. **102**: p. 215-219.

43. Schuch, R.F.V.A., *The Secret Life of the Anthrax Agent Bacillus Anthracis: Bacteriophage-Mediated Ecological Adaptations.* PLos One, 2009. **4**(8): p. e6532.

44. Adam, G. and M. Delbruck, *Reduction of dimensionality in biological diffusion processes*, in *Structural Chemistry in Molecular Biology*, A.D. Rich, N., Editor 1968, Freeman: San Francisco. p. 198-215.

45. Berg, H.C. and E.M. Purcell, *Physics of chemoreception.* Biophysical Journal, 1977. **20**(2): p. 193-219.

46. Alexrod, D. and M.D. Wang, *Reduction of dimensionailty kinetics at reaction-limited cell surface receptors.* J. biophys, 1994. **66**: p. 588-600.

47. Ricagno, S., et al., *Crystal Structure of the Receptor-binding Protein Head Domain from Lactococcus lactis Phage bIL170.* Journal of virology, 2006. **80**(18): p. 9331-9335.

48. Dupont, K., et al., *Identification of the receptor-binding protein in 936-species lactococcal bacteriophages.* Applied and environmental microbiology, 2004. **70**(10): p. 5818-5824.

49. Veesler, D., et al., *Crystal structure of Bacillus subtilis SPP1 phage gp22 shares fold similarity with a domain of lactococal phage p2 RBP.* Protein structure report, 2010. **19**: p. 1439-1443.

50. Tang, L., et al., *Three-dimensional structure of the bacteriophage P22 tail machine.* The EMBO jounrnal, 2005. **24**: p. 2087-2095.

51. Scholl, D., et al., *Bacteriophage K1-5 encodes two different tail fiber proteins, allowing it to infect and replicate on both K1 and K5 strains of Escherichia coli.* Journal of virology, 2001. **75**: p. 2509-2515.

52. Walter, M., et al., *Structure of the Receptor-binding protein of Bacteriophage Det7: a Podoviral Tail Spike in a Myovirus.* Journal of virology, 2008. **82**(5): p. 2265-2273.

53. Bartual, S.G., et al., *Structure of the bacteriophage T4 long tail fiber receptor-binding tip.* Proceedings of the National Academy of Sciences of the United States of America, 2010. **107**(47): p. 20287-20292.

54. Kawaura, T., et al., *Contributions of Polysaccharide and Lipid Regions of Lipopolysaccharide to the Recognition by Spike G Protein of Bacterophage X174.* Biosci. Biotechnol. Biochem., 2003. **67**(4): p. 869-876.

55. Abrescia, N.G., et al., *Insights into virus evolution and membrane biogenesis from the structure of the marine lipid-containing bacteriophage PM2.* Mol. Cell, 2008. **31**(5): p. 749-761.

56. Geller, B.L., et al., *Lactococcal 936-species phage attachment to surface of Lactococcus lactis.* J Dairy Sci, 2005. **88**(3): p. 900-907.

57. Archibald, A.R., et al., *Cell wall composition and surface properties in Bacillus subtilis: anomalous effect of incubation temperature on the phage-binding properties of bacteria containing veried amounts of teichoic acid.* J. gen. microbiol, 1989. **135**(3): p. 667-673.

58. Raisanen, L., et al., *Characterization of Lipoteichoic Acids as Lactobacillus delbrueckii Phage Receptor Components.* Journal of bacteriology, 2004. **186**(16): p. 5529-5532.

59. Baptista, C., M.A. Santos, and C. Sao-Jose, *Phage SPP1 reversible adsorption to Bacillus subtilis cell wall teichoic acids accelerates virus recognition of membrane receptor YueB.* Journal of bacteriology, 2009. **191**(5): p. 1726.

60. Sao-Jose, C., C. Baptista, and M.A. Santos, *Bacillus subtilis operon encoding a membrane receptor for bacteriophage SPP1.* Journal of bacteriology, 2004. **186**(24): p. 8337-8346.

61. Davison, S., et al., *Identification of the Bacillus anthracis (gamma) phage receptor.* Journal of bacteriology, 2005. **187**(19): p. 6742-9.

62. Ash, C., et al., *Comparative Analysis of Bacillus anthracis, Bacillus cereus, and Related Species on the Basis of Reverse Transcriptase Sequencing of 16S rRNA.* Intl Journal of Systematic Biology, 1991. **41**(3): p. 343-346.

63. Inglesby, T.V., et al, *Anthrax as a Biological Weapon, 2002: Updated Recommendations for Management.* JAMA, 2002. **287**: p. 2236-2252.

64. Turnbull, P.C.B., *Guidelines for the surveillance and control of anthrax in humans and animals*, W.H. Organization, Editor 1998.

65. LaForce, F.M., *Anthrax.* Clinical Infectious Diseases, 1994. **19**: p. 1009-1014.

66. Schuch, R., D. Nelson, and V.A. Fischetti, *A bacteriolytic agent that detects and kills Bacillus anthracis.* Nature, 2002. **418**: p. 884-889.

67. Edwards, K.A., H.A. Clancy, and A.J. Baeumner, *Bacillus anthracis: toxicology, epidemiology and current rapid-detection methods.* Anal Bioanal Chem, 2006. **384**: p. 73-84.

68. Choudhury, B., et al., *The Structure of the Major Cell Wall Polysaccharide of Bacillus anthracis is Species-specific.* Journal of Biological Chemistry, 2006. **281**(38): p. 27932-27941.

69. Mesnage, S., et al., *Bacterial SLH domain proteins are non-covalently anchored to the cell surface via a conserved mechanism involving wall polysaccharide pyruvylation.* EMBO J, 2000. **19**(17): p. 4473-4484.

70. Kern, J., et al., *Bacillus anthracis surface-layer proteins assemble by binding to the secondary cell wall polysaccharide in a manner that requires csaB and tagO.* Journal of Molecular Biology, 2010. **401**(5): p. 757-775.

71. Mignot, T.M., S.; Couture-Tosi, E.; Mock, M.; Fouet, A., *Developmental switch of S-layer protein synthesis.* Molecular microbiology, 2002. **43**(6): p. 1615-1627.

72. Raz, A. and V.A. Fischetti, *Sortase A localizes to distinct foci on the Streptococcus pyogenes membrane.* Proceedings of the National Academy of Sciences of the United States of America, 2008. **105**(47): p. 18549-54.

73. Fornelos, N., *Personal communication*, S. Kan, Editor 2011: via e-mail.

74. Daugelavicius, R., J.K. Bamford, and D.H. Bamford, *Changes in host cell energetics in response to bacteriophage PRD1 DNA entry.* Journal of bacteriology, 1997. **179**: p. 5203-5210.

75. Bamford, D.H., *Personal communication*, 2006: New York.

76. Kauder, S., S. Kan, and V.R. Racaniello, *Age-dependent poliovirus replication in the mouse central nervous system is determined by internal ribosome entry site-mediated translation.* Journal of virology, 2006. **80**(6): p. 2589-2595.

77. Kauder, S. and V.R. Racaniello, *Poliovirus tropism and attenuation are determined after internal ribosome entry.* J Clin Invest, 2004. **113**(12): p. 1743-1753.